Open your mind. LUT.
Lappeenranta University of Technology

Permanent Magnet Rotor Optimization

Otto Suuronen

M.Sc. thesis
LUT University
Electrical Engineering

24 June 2019

ABSTRACT

Lappeenranta University of Technology
LUT School of Energy Systems
Electrical Engineering

Otto Suuronen
Permanent Magnet Rotor Optimization

2019

Master's thesis.
62 pages, 48 figures and 10 tables.

Examiners: professor Juha Pyrhönen
Janne Nerg

Keywords: permanent magnet, FEA, rotor surface magnet, embedded magnet rotor, torque ripple, demagnetization

In this thesis different embedded magnet rotors are designed for a 10.4 MW wind turbine's permanent magnet synchronous generator which originally has a surface-magnet rotor. Their manufacturing cost, efficiency and operating properties are compared.

The study starts with a literary review of surface magnet and embedded magnet rotor properties. Pros and cons of the surface magnet and the embedded magnet rotor configurations are studied. After literary review, three different embedded magnet rotor structures are introduced and compared for further development. The rotor types are named based on the magnet layouts, which are radially embedded magnets, tangentially embedded magnets and two magnets per pole in V-position. The properties, that contribute to the machine properties are studied, too. Then the study continues with designing of an embedded magnet rotor. In the design process finite-element analysis (FEA) is utilized and the process consists of rated load, short circuit and no-load operation analysis. First, different magnet grades with different remanence and coercive force are compared from the cost point of view. Second, torque ripple is decreased with suitable magnet width, slot wedges, air gap length, skewing and rotor surface shaping. Third, efficiency is optimized to fulfil the required value. In efficiency optimization slot wedges, air gap length and shape and magnet segmentation are considered. Then, both two- and three-phase short circuits and demagnetization are analysed. Finally, no load operation is simulated, and analysed, and synchronous inductances are calculated.

During the design process, the radially embedded magnets rotor was abandoned in an early phase because it needs a high amount of magnets. The other two layouts succeeded all the way to the short circuit tests. The demagnetization analysis pointed out that rotor with two magnets per pole in V-position could not tolerate short circuits well whereas with tangential layout there should be no danger of demagnetization. All the analyses, that were done, show, that the tangentially embedded magnets rotor offers the best properties with the highest efficiency and pull-out torque without danger of demagnetization at short circuit.

TIIVISTELMÄ

Lappeenrannan Teknillinen yliopisto
LUT School of Energy Systems
Sähkötekniikka

Otto Suuronen
Kestomagneettiroottorin optimointi

2019

Diplomityö.
62 sivua, 48 kuvaa and 10 taulukkoa.

Tarkastajat: professori Juha Pyrhönen
Janne Nerg

Hakusanat: kestomagneetti, FEA, pintamagneettiroottori, uppomagneettiroottori, vääntöväre, demagnetoituminen

Diplomityössä suunnitellaan uppomagneettiroottori 10.4 MW tuuliturbiinin kestomagneettitahtigeneraattoria varten. Alun perin generaattorissa on pintamagneettiroottori. Työssä verrataan roottoreiden tuotantokustannuksia ja ominaisuuksia.

Työ alkaa kirjallisuuskatsauksella, jossa tutustutaan uppo- ja pintamagneettiroottoreiden ominaisuuksiin. Kirjallisuuskatsauksessa tutustutaan uppo- ja pintamagneettiroottoreiden hyviin ja huonoihin puoliin. Kirjallisuuskatsaukseen perustuen esitellään kolme uppomagneettiroottorityyppiä ja vertaillaan niitä jatkokehitystä varten. Roottorityypit on nimetty magneettiasetelmien perusteella ja ne ovat radiaalinen, tangentiaalinen ja V-muoto. Lisäksi tutustutaan ominaisuuksiin, jotka vaikuttavat generaattorin toiminta-arvoihin. Kirjallisuusosion jälkeen työ jatkuu uppomagneettiroottorin suunnittelulla. Suunnitteluprosessissa hyödynnetään numeerisiin menetelmiin perustuvaa analyysia (FEA) ja prosessi koostuu kuormitus-, oikosulku- ja tyhjäkäyntitilan analyyseistä. Ensimmäisenä vertaillaan kustannusnäkökulmasta koersiivivoiman ja remanenssin suhteen erilaisia magneettilaatuja. Toisena vääntövärettä pienennetään etsimällä sopivaa magneetin leveyttä, urakiilaa, ilmavälin pituutta, napojen vinoutusta ja roottorin pinnan muotoilua. Kolmantena optimoidaan hyötysuhde täyttämään vaadittu raja-arvo. Hyötysuhteen optimoinnissa tarkastellaan urakiilojen, ilmavälin pituuden ja muodon sekä magneettien segmentoinnin vaikutuksia. Seuraavaksi analysoidaan kaksi- ja kolmivaiheoikosulut sekä mahdolliset demagnetoitumat. Lopuksi simuloidaan ja analysoidaan koneen tyhjäkäyntiä sekä lasketaan tahti-induktanssit.

Suunnitteluprosessin aikana radiaalinen magneettiasetelma hylättiin hyvin aikaisessa vaiheessa suuren magneettimateriaalin tarpeen takia. Kaksi muuta roottorityyppiä selviytyivät oikosulkutesteihin asti. Demagnetoitumien analysointi osoitti, että V-muotoinen asetelma ei siedä hyvin oikosulkutilanteita, kun taas tangentiaalisella asetelmalla ei pitäisi olla demagnetoitumisen vaaraa. Kaikki tehtävät analyysit osoittavat, että tangentiaalinen asetelma tarjoaa parhaat ominaisuudet korkeimmalla hyötysuhteella ja kippivääntömomentilla ilman demagnetoitumisen vaaraa.

CONTENTS

LIST OF SYMBOLS AND ABBREVIATIONS

FEA	Finite Element Analysis
EMF	electromotive force
mmf	magnetomotive force
NdFeB	Neodymium-iron-boron
PM	Permanent Magnet
PMSM	Permanent Magnet Synchronous Machine
PWM	pulse-width-modulation
SRF	segmentation reduction factor

A	linear current density
B	magnetic flux density
$\cos\varphi$	power factor
E	electromotive force
f	frequency
F_{m}	magnetomotive force
H	magnetic field strength
h	height
I	current
k_{w}	winding factor
l	length
L	inductance
m	division split
n	division split
N	number of winding turns
p	number of pole pairs
P	power
Q	number of stator slots
S	apparent power
T	torque
U	voltage
V	volume
w	width

Θ	current linkage
ϕ	flux
μ	permeability
ψ	flux linkage
$\sigma_{F\text{tan}}$	tangential stress
ω	angular frequency
θ	angle
τ	pitch

Subscripts

c	coercivity
d	d-axis
cog	cogging
ec	eddy current
k	short circuit
m	magnetic
n	nominal
p	pole
ph	phase
PM	permanent magnet
p-p	peak-to-peak
q	q-axis
r	remanence, relative, rotor
rms	root-mean-square
s	stator, slot

δ	air gap

1. INTRODUCTION

Permanent magnet synchronous machines (PMSM) are very popular in a wide power range. PMSMs are rotating field machines. The rotor rotates along with the common magnetic field. Other rotating field machine types are other synchronous machines and induction machines. Synchronous machine rotor rotates with the same speed as the common magnetic field whereas the induction machine, also called as asynchronous machine, has a slip. In other words, induction machine's rotor runs asynchronously with different speed than the common magnetic field.

In order to rotate a rotor of an electrical machine, either mechanical (generator) or electrical (motor) energy is needed. As all electrical machines, a synchronous machine needs to be excited to forward the energy from rotor to stator or vice versa. Synchronous machine excitation can be implemented with stator winding or, especially, rotor field winding or with rotor permanent magnets (PM). Principally the rotor has dc magnetization. When the rotor of a synchronous generator is forced to rotate, the stator experiences an alternating magnetic field. A magnetic flux is produced by the rotor excitation and the flux circulates through the main magnetic circuit. The magnetic circuit consist of stator teeth, stator yoke, air gap, rotor yoke and permanent magnets in case of PM-machine. The direction of the flux is determined by the magnetization direction of the magnets. The poles next to each other are magnetized into opposite directions. While an alternating flux circulates through the magnetic circuit, it induces a voltage in the stator winding. According to Lenz's law, the possibly resulting current directs so that its flux tries to prevent the flux produced by the rotor from changing. As a result, there is a force that tries to prevent the rotation of the rotor creating a braking torque. The magnitude of induced voltage *e* can be calculated by using the applied form of the Faraday's induction law

$$e(t) = -\frac{\mathrm{d}\psi(t)}{\mathrm{d}t} = -k_{\mathrm{w1}} N \frac{\mathrm{d}\phi_{\mathrm{m}}(t)}{\mathrm{d}t}, \tag{1.1}$$

where ψ is the magnetic flux linkage, k_{w1} the fundamental winding factor, N the number of turns in a coil, t is time and ϕ_{m} is the magnetic flux. While the rotor is rotating, it produces sinusoidally alternating voltages in the stator winding, at least in principle. Practically, waveforms are not fully sinusoidal because of some harmonic content. There are lots of parameters that can be modified to shape the waveforms. For example, magnet dimensions, different winding solutions, air gap length and rotor pole shape can be modified to make the machine produce more sinusoidal voltage and less torque ripple.

The rotational speed n, pole pair number p and stator feed frequency f are depending on each other. The relation between these parameters is (Pyrhönen, et al, 2008)

$$f = \frac{pn}{60}. \tag{1.2}$$

Equation (1.2) emphasizes the fact that when a magnetized rotor rotates, it generates an electromotive force (EMF) in the stator windings. The frequency is defined by the rotational speed and the pole number ($2p$).

The sizing of a PMSM starts from defining the output torque. Torque T is related to the rotor volume V_r and $\sigma_{F\tan}$ which is the air-gap tangential stress caused by the electro-magnetic forces

$$T = 2\sigma_{F\tan}V_r. \tag{1.3}$$

where the tangential stress is defined as

$$\sigma_{F\tan} = AB_\delta \cos\gamma, \tag{1.4}$$

where A is the linear current density, B_δ the air gap flux density and $\cos\gamma$ an internal power factor describing the displacement between the air-gap flux density distribution and the linear current density distribution. In air-cooled PMSMs the tangential stress typically varies between 20 kPa and 50 kPa but can be increased with better cooling solutions and slower speeds (Pyrhönen, et al, 2008).

After choosing the dimensions of the rotor, air gap length should be decided. As a PMSM excitation cannot be controlled the synchronous inductance of the machine must be selected suitably to enable high enough peak torque. The peak torque is inversely proportional to the synchronous inductance (see eq. 1.5) which again is inversely proportional to the effective air gap length. Within the peak-torque boundary condition the air gap length should be minimized to save in the amount of magnets, but one must keep in mind that the shorter the air gap is the higher the effects of harmonics will be, and as a result losses increase, too.

The minimum physical air gap length is dictated by the mechanical constraints. A first magnet height h_{PM} can be estimated to be 5-10 times the physical air gap length δ_{mech}. The magnetic air gap of a rotor surface magnets machine $\delta_{em} \approx h_{PM} + \delta_{mech}$. Magnet height can be increased to prevent demagnetization of the magnet, if necessary. Standard magnets are usually square shaped to ease handling and assembly. As for choosing the correct magnet grade, the remanence, coercivity and temperature rating should be carefully considered and the balance between remanence and coercivity must be found. Coercivity and remanence are temperature dependent. Their values are usually given at room temperature, but the values are degraded in the nominal point operation of the machine as the temperature rises. Therefore, the worst-case demagnetization fields appear during possible short circuits while the machine is hot. The highest short circuit torques, however, appear while the machine is cold. Other important magnet properties are price, electrical conductivity and corrosivity. These are the properties that one would like to minimize. (Hendershot, et al, 2010)

The correct winding type is very much depending on machine type and application. Windings of a PMSM are usually divided in three phases and the magnetic pitch angle between phases is thus 120 electrical degrees. Winding of one phase consist of coils which have N conductor turns. Conductors are connected in series, to produce high enough voltage, and in parallel, to achieve suitable current density. Coils are placed in stator slots and the pitch between the coil sides is around 180 electrical degrees from one another depending on the winding step used. Anyway, coils are very often wound with a short pitch, where the pitch is for example 5/6 of the full pitch corresponding to 180 degrees. This is done to eliminate harmonics, but it will also reduce the induced emf (Hendershot, et al, 2010). In case of a tooth-coil winding, coils can be wound around every tooth (double-layer) or just every second (single-layer winding). Windings can be even toothless for example in ultrahigh-speed machines. A toothless winding has only a stator yoke. The cross-sectional

area of an individual conductor strand used in windings varies depending on the machine frequency. Higher frequency needs thinner conductor strands to avoid the adverse effects of skin effect. Anyway, skin effect is always present in the windings even in low-frequency machines. For high-frequency machines Litz wire may be utilized which has multiple thin strands in parallel. Litz wire and Roebel bar are good choices for preventing circulating currents because the conductors are transposed. Roebel bars are used in medium- and high-voltage machines. Transposing effectively cancels circulating currents caused by the alternating flux which is produced by current carrying conductors (Pyrhönen, et al, 2008). Skin effect and circulating currents are taken into account when AC resistance of the conductors is calculated. Resistance is also temperature dependent.

In the design of iron parts of the magnetic circuit, rotor and stator, one must dimension flux path cross-sectional areas so that flux densities remain low enough. The flux density should be kept under 1.5 T to avoid saturation but with low frequency machines this limit can be overrun without increasing iron losses severely. Saturation increases the mmf of the system and results in a high need of excitation current linkage. Areas of stator iron parts can be designed based on flux density values on stator teeth and stator yoke. The pole number ($2p$) influences the needed stator yoke thickness, since a high pole number results in a small main flux per magnetic circuit. Winding type also contributes to the stator iron design by defining the number of slots. In stator tooth tip design, saturation should be considered, too. Too thin or tapered tooth tip is liable to saturate, and it easily increases torque ripple similarly as too wide slot opening. Stator iron parts are made from thin, high resistivity laminations to decrease losses because of alternating flux. Usually lamination thicknesses vary from 2 mm to 0.5 mm, but even thinner laminations may be needed with high-speed machines. Rotor can be made of solid iron because of dc magnetization. Though, air gap flux density has harmonic components that cause losses and therefore rotor is usually made of thin laminations to achieve maximal efficiency. (Hendershot, et al, 2010)

The operation of synchronous machines is determined by its direct (d) and quadrature (q) axis inductances (Pyrhönen, et al, 2008). The d-axis is in the direction of rotor pole and the q-axis is between poles. If the rotor is of non-salient pole type, it has, in principle, equal inductances on both axes whereas a salient pole rotor has difference between the synchronous inductances. The reason for this is that d- and q-axes have different equivalent air gap lengths. So, stator inductance varies as a function of rotor position. The load angle equation is

$$P = 3\left(\frac{U_{\mathrm{ph}}E_{\mathrm{f}}}{L_{\mathrm{d}}\omega_{\mathrm{s}}}\sin(\delta) + U_{\mathrm{ph}}^2\frac{L_{\mathrm{d}}-L_{\mathrm{q}}}{2\omega_{\mathrm{s}}L_{\mathrm{d}}L_{\mathrm{q}}}\sin(2\delta)\right), \qquad (1.5)$$

where P is the power, U_{ph} the phase voltage, E_{f} the phase electromotive force, L_{d} the d-axis synchronous inductance, L_{q} the q-axis synchronous inductance, δ the load angle and ω_{s} the electrical angular velocity (Pyrhönen, et al, 2008). L_{d} and L_{q} consist of magnetizing part $L_{\mathrm{md,q}}$ and leakage part L_{σ}. Torque is got from equation (1.5) by dividing the power with mechanical angular velocity ω_{s}/p. The first part of (1.5) is called the excitation power and the latter the reluctance power. From the load angle equation, it is seen that when the synchronous inductances are equal, the machine does not produce reluctance torque. Equation (1.5) also points out that when the load angle is 135°, the reluctance torque has its maximum value in machines with inverse saliency ($L_{\mathrm{q}} > L_{\mathrm{d}}$), also known as pull-out point, whereas non-salient pole machine has its maximum torque at load angle 90°. PMSMs with embedded magnet design usually have their pull-out torque between 90° and 135°. Practical operating load

angle is lower to maintain torque reserve. D- and q-axis and salient and non-salient pole rotors are presented in the figure 1.1.

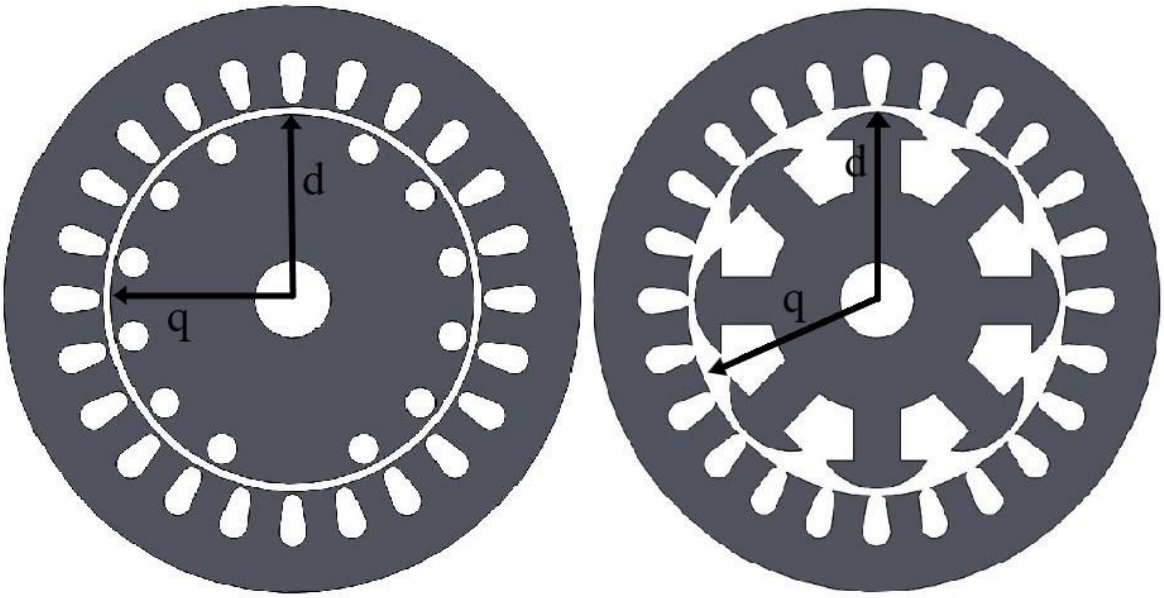

Figure 1.1 Non-salient pole machine (two-pole) on the left and salient pole machine (eight-pole) on the right. Examples of possible d- and q-axis positions are marked in the figure. In case of a non-salient pole machine the d-axis is fixed on the field-winding magnetic axis. In PMSMs the d-axis is fixed to the permanent magnet current linkage axis.

Inductances are very important to electrical machines and they have many notable effects on machine operation. The d- and q-axis steady state equivalent circuits of a synchronous machine are presented in figure 1.2. Equivalent circuits have only synchronous inductance components in steady state. Equivalent circuits for different transient states can be studied for example from Pyrhönen, et al, (2008). Synchronous inductance limits the sustained short circuit currents. It also affects the power factor, pull-out torque and operation at over speed, which is also called as field weakening operation. Too high inductance gives a low pull-out torque. The armature reaction, that distorts the flux of the magnets, is also produced by inductance. With high enough inductance, armature reaction can be used to reduce PM flux to be able to run the machine faster. (Hendershot, et al, 2010)

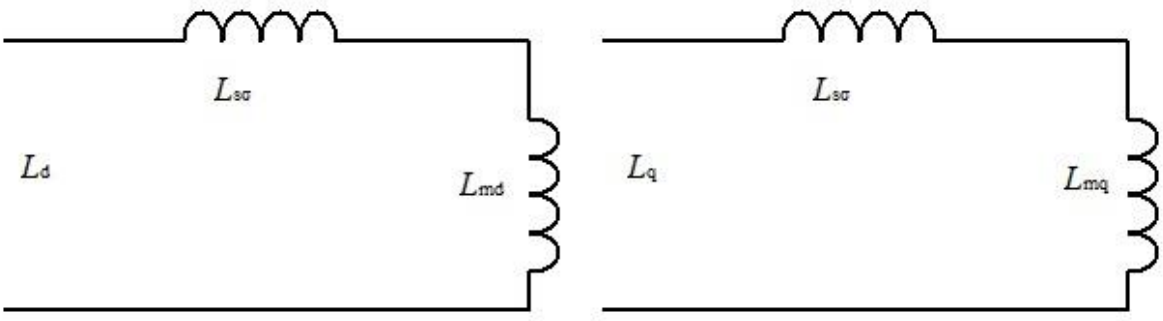

Figure 1.2 Steady state equivalent circuits of a synchronous machine for both d- and q-axis (Pyrhönen, et al, 2008). Equivalent circuit have only components that form the synchronous inductance, magnetizing and leakage inductance components.

Electrical machines have also lots of different leakage flux components that form leakage inductances, slot leakage, tooth tip leakage, pole leakage and end-winding leakage inductance. Leakage inductances suppress the main flux and produce leakage fluxes that do not participate in electromagnetic energy conversion. Leakage fluxes are not directly associated with losses. They are often thought to be negative phenomenon, but they have also positive effects like filtering pulse-width-modulated (PWM) supply and preventing the demagnetization of the PMs. (Pyrhönen, et al, 2008)

Permanent magnets are used for machine excitation since they provide higher efficiency than electrically exited machines because of, in principle, lossless excitation. PMSMs provide also higher torque and power density, meaning that a PM-machine can produce the same power as an electrically exited machine with a lower volume. PMSMs are also maintenance free since they have neither slip rings nor other wearing parts except bearings. A very beneficial feature in PM-machines in comparison with other machine types is that they can offer a high efficiency with a wide range of speeds (Gieras, et al., 1997). These reasons explain why PM machines are very popular in all kinds of application where the rotational speed varies, high efficiency is needed and size matters. The biggest drawback of the machine type is its high price. The main reason for the high price of these machines is the high price of rare earth magnets needed in the excitation. Easily recoverable reserves of materials needed in the PMs are accumulated in small geographical areas. Total reserves are not very high and very high amount of the easily recoverable reserves belong to China, thus they have very a high effect on the price of PMs.

There are also some vulnerabilities related to the permanent magnets. Finally, grades used in high-power machines are not lossless but may have significant eddy current losses and, in some unfortunate cases also hysteresis losses. They do not usually tolerate as high operating temperatures as windings do. There are, however, some SmCo magnet grades offering even 300 °C maximum operating temperature. It is possible to lose the polarization of a permanent magnet under certain demagnetizing conditions. These conditions have to be taken carefully into account when designing a permanent-magnet-excited synchronous machine.

1.1 Study Background – Rotor Types

There are a few different basic mounting types for magnets when we are considering internal rotor radial flux PM machines. The mounting types are rotor-surface-mounted magnets, magnets inset on the surface, magnets mounted under pole shoes, magnets embedded tangentially or radially in the rotor core, two magnets constructing a pole in the V-position and a synchronous reluctance rotor equipped with PMs. All different rotor configurations have their advantages and disadvantages. This thesis concentrates on replacing a surface magnet rotor construction with an embedded magnet rotor construction. Thus, only these types are discussed hereafter.

One beneficial thing in the rotor surface magnets rotor is that it utilizes very large share of the PM's flux in the excitation, so minimum amount of magnet material is needed (Pyrhönen, et al., 2008). However, rotational speed must be low enough to keep the magnets fixed on the rotor surface. If the speed is too high, magnets will disengage from the rotor surface due to centrifugal force. In all cases, the magnets must be fastened on the rotor surface with complex mechanical structures or glue.

Embedded magnet designs have a disadvantage that the rotor needs more magnet material than a rotor surface magnets version, which increases the price of the machine (Pyrhönen, et al., 2008). Anyway, this construction type suits better for higher rotational speeds since the magnets are inside the rotor and thus, they are protected against the centrifugal force. Thus, embedded magnet rotor construction is studied to be able to run the machine with higher speeds and scale the machine bigger for the future designs.

1.2 Objectives

The target of the thesis is to study whether it is possible to design the rotor of a PM generator with embedded magnet design cost efficiently or not, when it is compared with a rotor surface magnets design. In the thesis, embedded magnet design is made for The Switch PMM1500 wind turbine generator which originally is built with rotor surface magnets. The performance improvements and price change of the embedded magnet design in comparison with the rotor surface magnet design is studied. To achieve a solution for the main target, features affecting the rotor performance are to be studied. The final solution should be high enough performance and efficiency with reasonable price increase compared to the original rotor surface magnet design.

Usually, electrical machine design follows a predestined procedure. PMSM design process can include the following phases (Puranen 2015):

- set of the initial design parameters, rated speed and power
- selecting rotor dimensions, air gap length and calculating magnet thickness
- selecting the number of stator slots and poles
- selecting the winding type, calculating the number of turns per coil and wire dimensions
- selecting and calculating the current densities and flux densities in the stator and rotor
- selecting skewing angle of the magnets.

In this case the stator structure, rotational speed, the number of poles and power are already decided. So, only the rotor structure is modified. The output power that is aimed for is 10.4 MW. To find out the machine behaviour, finite element analyses (FEA) are done. Different computations are carried out to find out the behaviour of the following properties:

- air gap flux density and its spectrum at no-load and full load
- flux densities in stator yoke and teeth at no-load and full load
- synchronous inductances
- 2- and 3-phase short circuit torques (cold machine parameters)
- 2- and 3-phase short circuit currents (cold machine parameters)
- risk of demagnetization at 2- and 3-phase short circuit (hot machine parameters)
- torque ripple at no-load and full load (at rated temperature)
- losses in rotor and stator core, magnets and copper (at rated temperature).

1.3 Research Methods

In the beginning, a short literature review is made to study the features that must be considered in the optimizing process of the rotor. The design criteria found in the literature are utilized in the design and in the optimizing process of the interior PM machine. After finding a plausible rotor design by literature review, the design is verified with finite element analysis.

1.4 Structure of the Thesis

The thesis is structured as in the following order. Firstly, the differences between rotor surface magnets and embedded magnet designs are studied. Secondly, the properties that should be considered during optimization process are discussed. Thirdly, the machine modelling at rated torque is done. Then, maximum torque is found out and short circuit and no load situations are analysed. Finally, the results and conclusions of the modelling are done.

2. EMBEDDED MAGNET DESIGN

In this chapter the main features affecting the rotor behaviour and waveforms of the air gap flux density, back-EMF and torque are considered. The applicability of different magnet layouts, constructions and grades are thoroughly discussed as well as skewing, air gap length and slot wedges.

2.1 Benefits and Drawbacks

The benefits of both surface magnets and embedded magnets are different and therefore they are applicable for different applications. Probably the most beneficial feature of the embedded magnets is that a rotor equipped with embedded magnets can tolerate higher peripheral speeds than a rotor with surface magnets. The original PMM1500 has rotor surface magnets and is designed to withstand a peripheral speed of about 65 m/s. This speed is still moderate and can be achieved with a rotor surface magnets. Anyway, if the peripheral speed must be risen remarkably, the centrifugal forces increase, and a rotor surface magnets design might break down, if the clamping system stays the same. Therefore, an embedded magnet design may be a better choice for protecting the magnets fixing system against high mechanical stresses that magnets encounter at high speeds (Gieras, et al., 1997).

Rotor surface magnets need a clamping system to keep them on their correct places. The mechanical properties of the magnets themselves may also cause limiting boundary conditions because, in practice, sintered PM materials do not tolerate significant tensile stresses. Therefore, clamping a magnet on the surface with a method that, in principle, lets the magnet bend outwards as a result of centrifugal force, may result in cracking the magnet. Therefore, rotor surface magnets often need an assembly pocket or bandage made e.g. of stainless steel maintaining the form of the magnet under high centrifugal forces. Therefore, the design of a clamping system and the system itself may be very complex and requires very detailed analysis because of different material properties for example in thermal expansion and strength. The assembling process of rotor surface magnets is also very difficult because of high magnetic forces between magnets and between the magnets and the rotor yoke (Liimatainen 2015). An embedded magnet design does not have these drawbacks, since the magnets are placed inside the rotor in their own pockets and thus, not needing a very complex separate clamping system. In addition, controlling the magnetic forces during assembly seems much easier in case of embedded magnets than rotor surface magnets.

In rotor surface magnet machines, eddy current losses are created in magnets since sintered magnets are conductive. Typical conductivity of NdFeB magnets is in the range of 600 kS/m. When the frequency of the machine increases, also the losses typically increase. The frequency depends on the rotational speed and pole-pair number of the machine. Therefore, in rotor surface magnet design avoiding losses in permanent magnets must be considered

carefully (Pyrhönen, et al., 2008). In an embedded magnet design, magnets do not suffer of as high losses because slot and stator current linkage harmonics are attenuated in the rotor core. On the other hand, rotor surface magnets have better cooling encountering direct air cooling in the air gap while embedded magnets are located inside the rotor core and their effective cooling is, therefore, somewhat complicated. Because of this, embedded magnet design may need separate cooling channels to keep permanent magnets cool enough so that they do not become demagnetized during possible stator terminal short circuit (Liimatainen 2015). Cooling channels make a rotor structure complicated.

Rotor surface magnet machines are principally nonsalient-pole machines in which the ratio of d- and q-axis synchronous inductance is one. The reasons for this are that the rotor core is totally round, when magnets are mounted on the rotor surface, and the relative permeability of neodymium-iron-boron magnets is approximately one ($\mu_r \approx 1.04$), thus almost equalling that one of air. The saliency ratio of an embedded magnet design is somewhat different depending on the magnet arrangement, since the magnets are inside the rotor, which means that the machine operation is different. When magnets are inside the rotor, they bring inside the ferromagnetic core material that can apparently be seen as air. Therefore, an embedded magnet rotor becomes inversely salient meaning that the synchronous inductance of the q-axis is bigger than the one of d-axis. Saliency means that there will also be some reluctance torque present in the machine. (Pyrhönen, et al., 2008)

When magnets are embedded entirely inside the rotor structure, a substantial share of the flux produced by the magnets is wasted. The flux is wasted in the PM flux leakage components of the rotor. This phenomenon is illustrated in figure 2.1. Also, the magnet pole area inside the rotor is usually smaller than the pole area on the surface of the rotor, so that the air gap flux density is smaller than the flux density in the magnet (Gieras, et al., 1997). Therefore, more magnet material or magnets with higher remanent flux density is needed in an embedded magnet design to produce the same flux as with rotor surface magnets. On the other hand, in case where there are two magnets per pole there is a possibility to clearly increase the flux of the machine.

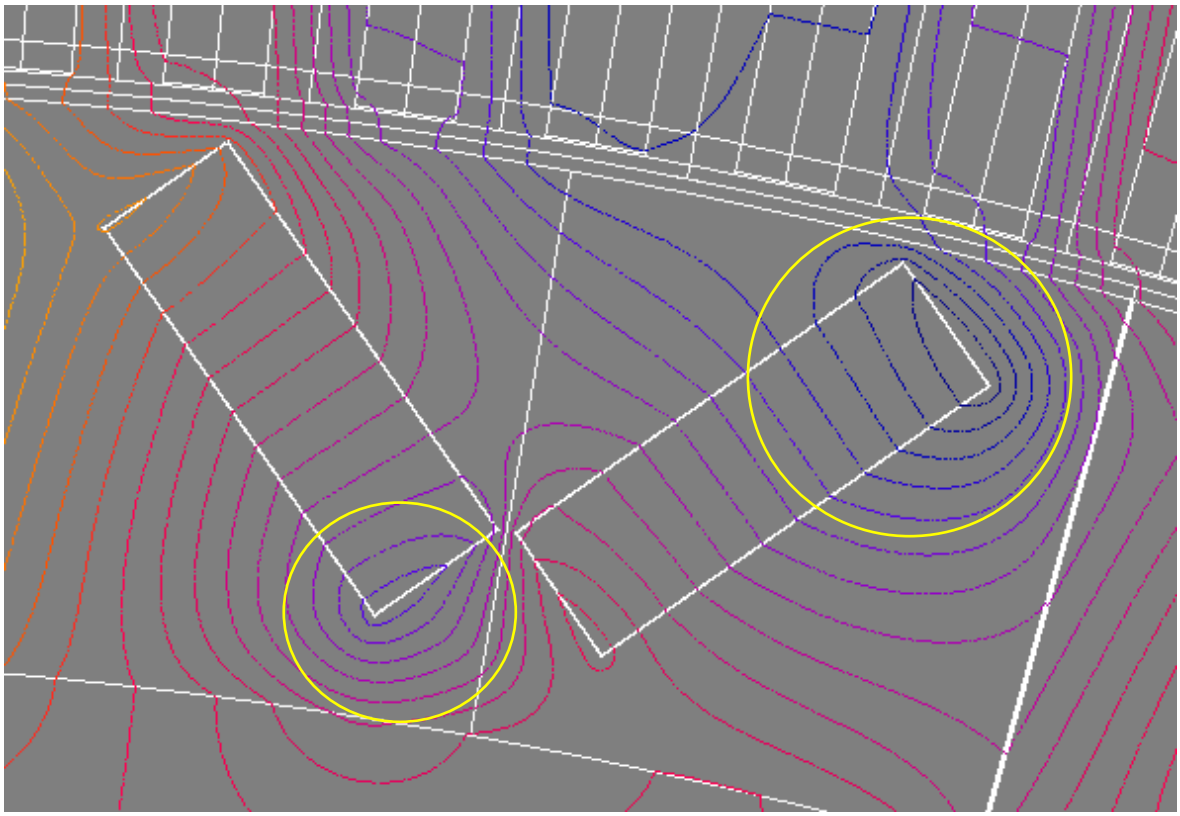

Figure 2.1 Flux leakage appears at magnet fringes (see especially yellow circled areas) and between magnets in a rotor with embedded magnets.

The magnitude of the synchronous inductance $L_{d,q}$ has a decisive effect on torque production. The lower the synchronous inductance is the higher is the ability of torque production. This can be seen in the load-angle equation (1.5) of the synchronous machine. The synchronous inductance is in the denominator. So, the highest torque production capability is got when the magnetic air gap length is high. This results from the inverse proportionality of inductance and reluctance, and air as a medium has a high effect on reluctance. Generally, a small air gap causes higher extra losses than a longer one due to harmonic content for example. So, changing to embedded magnets can reduce the torque production capability if the physical air gap is kept the same. (Pyrhönen, et al., 2008)

Even though the torque production capability of the PM machine will decrease, if it has embedded magnets instead of rotor surface magnets, the quality of the torque in most design cases is better (Wang, et al., 2011). The torque ripple may be decreased with embedded magnets, since they produce more sinusoidal waveforms, and this means that the harmonic content is reduced (Athanasopoulos, et al., 2016). Also, the efficiency of an embedded magnet machine is typically better than that of a rotor surface magnet machine (Lindh, et al., 2009).

2.2 **Permanent Magnet Layout**

The rotor construction defines the characteristics of a permanent magnet machine (Pyrhönen, et al., 2008). The layout of the magnets defines the air gap flux waveform characteristics and thus, torque characteristics and of course, also the rated power depends on the rotor construction. Aspects that contribute to machine design are mechanical, thermodynamic and electrical constraints.

In figure 2.2, there are three different magnet layouts that could offer possible solutions for a rotor construction. Each of them has its own advantages and disadvantages. The first rotor topology on the left has one radially set magnet per pole. This rotor type was developed to increase the air gap flux density by the flux concentration method. The magnets are circumferentially magnetized (Hendershot, et al, 2010). The flux concentration can be significant in multiple-pole machines where the radial width of the magnet can be significantly larger than the pole pitch of the machine. In some cases, even weaker magnet material might be used because of this feature. The d- and q-axis inductances of this structure have a significant difference and therefore the machine has an ability to produce some reluctance torque similarly as all the rotor types with embedded magnets. Radially embedded magnets structure may also need less magnet material than other embedded designs because of the possibly high reluctance torque contribution and thus, diminish the total cost of the machine. Although increasing the reluctance torque sounds attempting, it can easily increase the torque ripple and cogging torque as well (Hahlbeck, et al, 2008). It has also a higher back-EMF, torque and efficiency and lower torque ripple and cogging than any other inset PM-rotor types in study (Charih, et al, 2012). Athanasopoulos, et al., (2016) showed that the radial structure provides a high air gap flux density, harmonic values and cogging. The most significant disadvantage of the rotor type is that it needs a thicker and heavier rotor yoke. The behaviour of course depends on other aspects of the rotor and stator design, so the final suitability cannot be decided here without further analysis with for example with finite-element based analysis (FEA).

The rotor structure in the middle in figure 2.2 has tangentially embedded magnets having one magnet per pole. This structure offers a lower back-EMF, a lower torque, a lower efficiency and lower air gap flux density than the previous rotor type according to studies by Athanasopoulos, et al. (2016) and Charih, et al. (2012). Cogging torque of this rotor type is considered to be the smallest of the embedded magnet machine types in some research papers while others claim that it has the highest cogging. Also, in (Wang, et al, 2011) and (Vakil, et al, 2010) different results are presented for this rotor type. Yet again the rotor and stator structures have a significant effect on this quantity.

The last rotor structure on the right in figure 2.2 has two magnets per pole in V-position. This rotor type can offer a significant reluctance torque which can be further increase by arranging flux barriers on the d-axis. In basic design the proportions of PM and reluctance torque can be determined by the V-position. The angle between the magnets can, in principle, be any between 0°–180°. Two magnets per pole in V-position design produces a more sinusoidal air gap flux density waveform than the tangentially embedded magnet design and the flux density can be quite high since there are two magnets utilized per pole (Pyrhönen, et al, 2008). This rotor type provides a high power and torque on a wider speed range. Thus, two magnets per pole in V-position design suits well for a wide speed range but it usually offers a little lower nominal torque (Wang, et al, 2011).

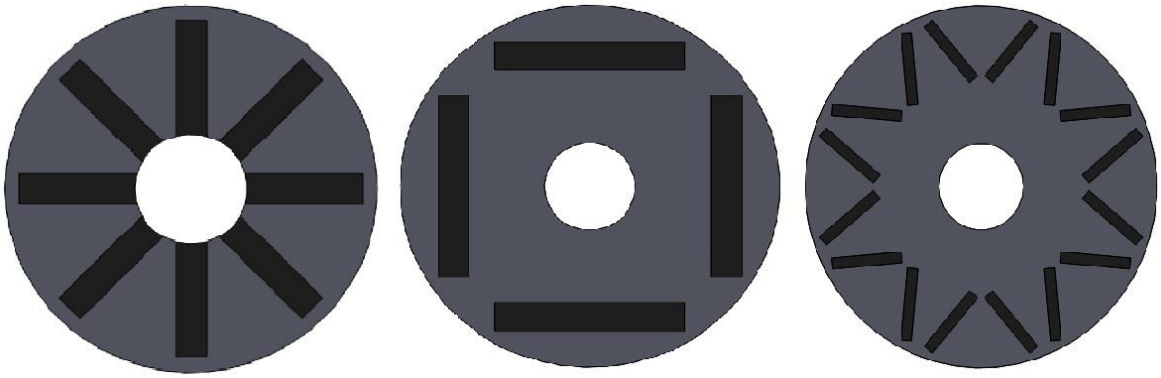

Figure 2.2 Different rotor topology proposals for the final design. The first one on the left has radially embedded magnets, the one in the middle has tangentially embedded magnets and the final one on the right has two magnets per pole in V-position. Topologies are redrawn based on information from Pyrhönen, et al. (2008).

2.3 **Permanent Magnet Grades**

The original PM-material used in the PMM1500 machine is neodymium-iron-boron (NdFeB) as it offers the highest coercivity available. There are different grades of NdFeB material in which the remanent flux density, operating temperature and price vary. The grades are labelled in form 40UH. 40 refers to the maximum energy product of the material in unit millions of Gauss Oersted (MGOe). Letters "UH" after the number tell the temperature rating of the material and is equivalent to 150 °C (K&J Magnetics Inc.) in this case.

NdFeB magnets are expensive and, hence the cost optimum must be found to minimize the costs but to keep the performance. As said earlier, the main differences between the magnet grades are remanence, operating temperature and price. A higher remanence and a higher operating temperature come with higher price. According to Ampere's law the magnetomotive force of a magnetic circuit equals the current linkage if the circuit

$$\oint \boldsymbol{H} \cdot \mathrm{d}\boldsymbol{l} = \Theta(t), \tag{2.1}$$

where $\boldsymbol{H}$ is the magnetic field strength, $\boldsymbol{l}$ the length of magnetic circuit and Θ the current linkage. Less magnet material is also needed to produce the desired air gap flux with higher remanence flux magnets. The magnetomotive force $\oint \boldsymbol{H} \cdot \mathrm{d}\boldsymbol{l} = F_\mathrm{m}$ (mmf), that the magnetic circuit needs. At no load, this mmf must be covered by the PM current linkages. If the machine has rotor surface magnets or embedded magnets the mmf is, in practice, covered by two magnets in series. Therefore, half of the mmf is covered by one magnet with its current linkage

$$\Theta_\mathrm{PM} = H_\mathrm{c} h_\mathrm{PM}, \tag{2.2}$$

where H_c is the coercive magnetizing force of the magnet and h_PM the height of the magnet. If there is just one single magnet e.g. in a two-pole machine, the whole mmf must be covered by the single magnet.

According to equation (2.2) a thinner magnet results in a smaller current linkage. Too high temperature because of losses or too high demagnetizing magnetic field strength because of a short circuit can lead into demagnetisation of permanent magnets. If the demagnetizing

field strength goes higher than the strength of coercive force in the polarization curve knee-point, irreversible demagnetization occurs. PM's coercive force and remanence decrease as the temperature rises, so demagnetization becomes easier. Examples of knee-points for different temperatures are depicted in figure 2.3. As stated earlier, the synchronous inductance has a high impact on torque production. So, if the magnet is too thin, the synchronous inductance is high, and the maximum torque is low. Such a machine operates too close to the pull-out point and may not have enough torque reserve. Low synchronous inductance is not good either in case of short circuit, since the current would rise too high.

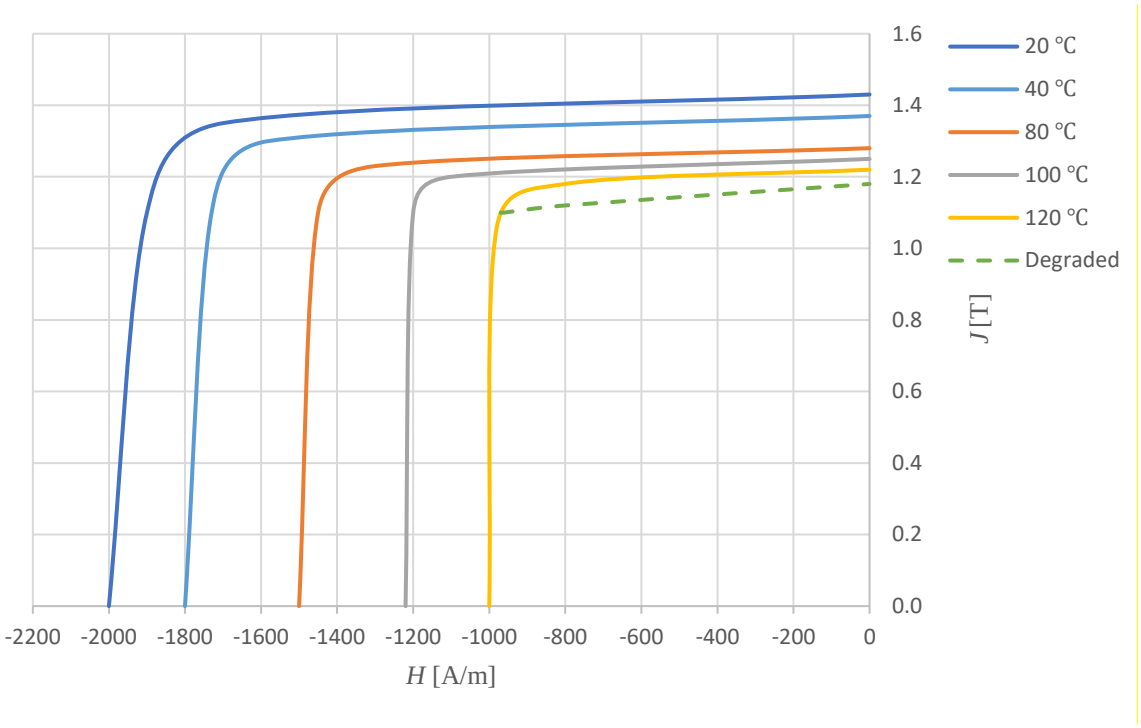

Figure 2.3 Example curves of a PM *JH* characteristics. Polarization knee curves for different temperatures. If demagnetizing field strength is higher than the coercive force in the knee point, then a new knee-point is set to the point where the demagnetizing field strength has proceeded. Then a new remanence flux value is defined by the new intersection of the knee curve and *J*-axis. This phenomenon is depicted in the figure with dashed line for the 120 °C curve.

For the optimization process, five magnet grades are chosen and both thickness and width for them are found. In the table below the grades chosen, their remanence (B_r) and price indices are listed. Table's values are based on information given by a PM supplier.

Table 2.1 Magnet grades chosen for the optimization process. Table contains also remanence fluxes and price indices of the magnet grades. Values are based on PM supplier's information.

	B_r [T]	Price index [%]
N42TH	1.28	100
G45UH	1.30	112
G48TH	1.36	115
G50UH	1.38	117
G52TH	1.40	111

2.4 Permanent Magnet Segmentation

Most of the losses in the permanent magnets of rotating electrical machines are produced by eddy currents. However, also hysteresis losses can be present, but in carefully designed machines they do not play a significant role (Pyrhönen, et al., 2015). The permanent magnets are conductive and, thus they provide a path for eddy currents and produce losses. Eddy current losses are proportional to the square of the frequency and inversely proportional to the material resistivity.

If big, solid magnets are used in a rotor, the magnets may encounter so high eddy current losses that they lose their polarization because of a high temperature (Pyrhönen, et al., 2015). To limit these losses in permanent magnets, the magnets can be segmented and segments isolated galvanically from each another, thus providing smaller and higher-resistance paths for eddy currents. This decreases the losses in permanent magnets. So, segmented individual magnets are built from small, for example 5 mm, slices. Segmentation decreases the eddy current paths and increases the effective resistivity of the magnets. In figure 2.4 this phenomenon is illustrated.

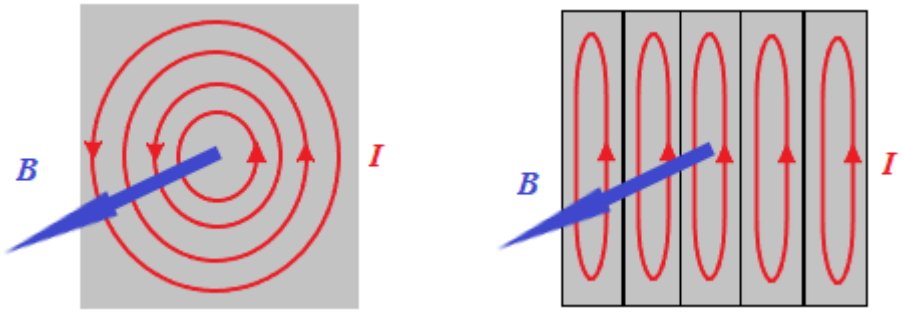

Figure 2.4 Eddy currents in big solid part and in smaller parts.

An ultimately simplified analysis of the reduction of eddy current losses is given here. If we consider a cross-sectional surface whose length is l and the pole-pitch of the exiting space harmonic is τ, and the induced emf proportional to the magnet cross-sectional surface normal to the flux is E, the eddy current path resistance is about proportional to $2(l+\tau)$ and the eddy current losses of the surface are about

$$P_{\mathrm{ec}} \sim \frac{E^2}{2(l+\tau)}. \tag{2.3}$$

If we then divide the surface into m divisions in τ direction and in n divisions in length l direction, the emf driving the eddy currents in each segment will be reduced to $E/(mn)$ and the sum of the eddy current losses of the segmented surface is

$$P_{\mathrm{ec,seg}} \sim mn \frac{\left(\frac{E}{mn}\right)^2}{2\left(\frac{l}{n}+\frac{\tau}{m}\right)}. \tag{2.4}$$

The ratio of eddy current losses in segmented and uniform (bulk) surfaces is

$$\frac{P_{\mathrm{ec,seg}}}{P_{\mathrm{ec}}} = \frac{l+\tau}{ml+n\tau}. \tag{2.5}$$

Let us consider that l is equal to τ and $m = n = 5$, the eddy current losses are reduced to 20 % of the original losses. In equation (2.5) it can be seen that the simple analysis of eddy current reduction is really very simple. However, precise calculation requires FEA. (Hendershot, et al, 2010)

2.5 **Skewing**

Stator or rotor skewing is often applied in machine design, since it has more positive than negative effects on machine behaviour. Skewing means that, for example on the rotor side, magnets of a pole are unaligned. So, in a non-skewed rotor, magnets of one pole form a straight line from one end of the rotor to another but in a skewed rotor, some magnets can be in tangentially different position. Skewing can be utilized with several different ways on the rotor side in PM machine. Magnets can be inserted in a few stages or all the magnets can be in different perimeter position. When designing skewing of the rotor, one must also consider what is feasible from the manufacturing point of view. A schematic illustration of a skewed rotor is given in figure 2.5.

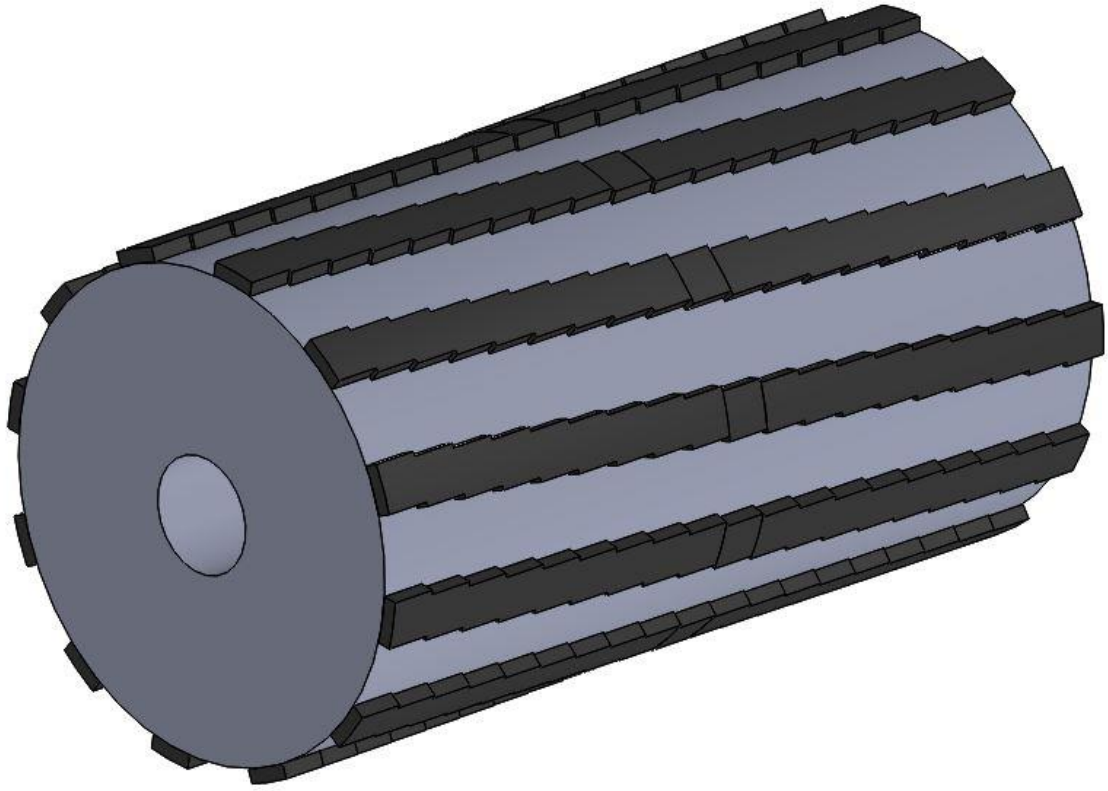

Figure 2.5 Skewed rotor principle applied to a rotor surface magnets design.

The main object of skewing is to reduce the effect of certain air gap harmonic components and therefore to make the torque of the machine smoother and to achieve less cogging. Skewing weakens the magnetic connection between the stator and the rotor and causes leakage fluxes. Therefore, skewing reduces the winding factor and the fundamental of emf by the skewing factor (Pyrhönen. et al., 2008). Overall design of the stator and rotor define the final behaviour of the machine and how much attenuation for the ripple and cogging is needed. For analysing the effects of skewing usually FEA is utilized.

According to (Zhao, et al, 2015), the best torque characteristics are achieved with symmetrical skewing and sinusoidal skewing methods. Also, the more steps skewing has the less cogging it will produce. The principles of these methods are depicted in figure 2.6.

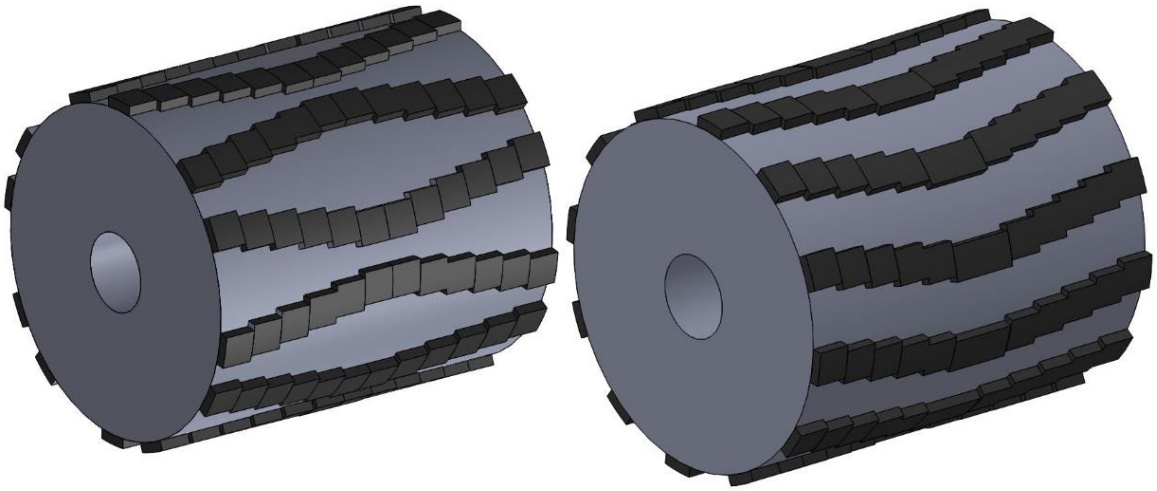

Figure 2.6 Skewing methods that produce the best torque characteristics. On the left, sinusoidal skewing and on the right, symmetrical skewing.

Based on (Zhao, et al, 2015), both abovementioned skewing methods produce very similar properties. However, sinusoidal skewing method requires different lamination structure at every step. So, manufacturing process becomes more difficult and more expensive. Thus, symmetrical skewing method is applied. The more skewing steps a rotor has, the more complex and expensive it becomes. So, two- and three-step skewings are studied. Skewing angle is often chosen to be one stator slot pitch, since it effectively cancels the effects of slot harmonics (Pyrhönen, et al, 2008).

2.6 **Air Gap**

As stated earlier the length of the magnetic air gap has a very important role. Air gap length affects the mmf of the magnetic circuit, because of air gap's large reluctance and therefore magnetic voltage in the magnetic circuit. Thus, the air gap length affects the flux of the machine very much. Air gap length is mainly defined by mechanics, but it has also impact on inductance, torque ripple and losses. A small air gap increases the losses on the rotor surface caused by the current linkage harmonics of the stator and therefore the air gap length is increased in some applications. A long air gap decreases the inductance and, thus increases the machine maximum torque. Air gap length is wanted to be minimized, because the longer it is the more magnet material is needed to produce the desired flux and the total price of the machine becomes higher. So, a compromise between the price and efficiency must be found.

Another means to reduce the torque ripple, is to shape the air gap so that d- and q-axis inductances are as close as possible to equal. So, d- and q-axes have different air gap lengths. In this case the reluctance torque is very small and torque ripple is decreased when compared with a fully round rotor. Air gap shaping affects the air gap flux density waveform and through it the emf, losses, efficiency and torque (Liu, et al, 2013).

2.7 **Slot Wedges**

Slot wedge design is taken into account in the optimization process, even though wedges exist on the stator side. They have a great impact on the air gap flux pulsation. The function of the slot wedge is to attenuate those pulsations by fading out the sharp corners of the stator teeth (Lindh, et al, 2013). Large machines are usually built with fully open stator slots and the slots are closed with a slot wedge. Slot wedges are inserted between stator teeth above a recess in a stator core in which the conductors of a winding are set. Figure 2.7 illustrates the positioning of a wedge.

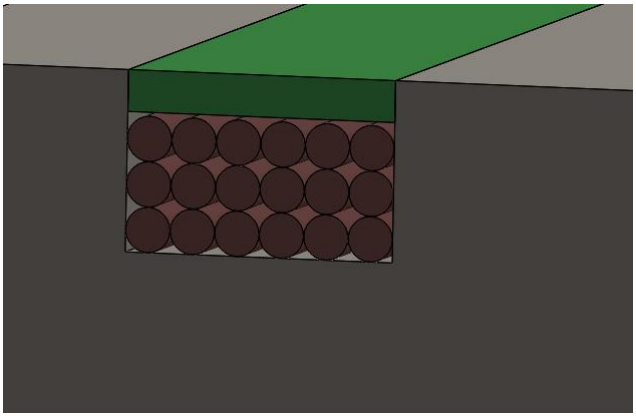

Figure 2.7 Illustrative figure of a slot wedge (green) insertion in a stator slot.

Slot wedges can be made of three kinds of materials – nonmagnetic ($\mu_r = 1$), semi-magnetic materials ($\mu_r = 1…10$) or soft magnetic composite ($\mu_r > 10$) (Lindh, et al, 2013). The advantages of magnetic wedges in comparison with nonmagnetic wedges are lower temperature rise, reduced core and magnet losses, a little bit higher machine efficiency and lower noise intensity. The drawback of magnetic wedges is that they are more brittle than nonmagnetic wedges because of the high proportion of iron powder in the structure and they decrease the pull-out torque of the machine. Magnetic wedges are also more expensive. (Hanna, et al, 2012) (Wang, et al, 2008)

Slot wedge material and thickness have a significant influence on the performance and characteristics of the machine. To obtain the maximum efficiency and power, the relative permeability of the slot wedge material should be between 5 and 10. With higher values of permeability, the pull-out torque drops abruptly because of the increased slot leakage via the slot wedges. The effects of slot wedge thickness are similar and optimal performance is got when the thickness is between 3 mm and 5 mm with typical wide high-power-machine slot opening widths. A thicker wedge means a larger area for the slot leakage flux to travel. This increases the leakage fluxes and decreases the main flux that contributes to torque production. (Wang, et al, 2008)

In order to achieve desired properties for the machine, optimal thickness and material for the slot wedge must be found. The optimal result is a compromise between the efficiency and the pull-out torque where cogging torque meets the limits and manufacturing is possible.

3. ROTOR LAMINATION DESIGN

The active parts of the rotor of a PMSM consist of permanent magnets and ferromagnetic laminated steel sheets where the main flux travels. Steel sheet areas close to rotor surface experience a fluctuating magnetic field and, thus, to minimize losses, the rotor is built from non-oriented electric sheets. In non-oriented electric sheets, the properties stay constant regardless of the direction the flux is travelling. The fluctuations of the magnetic field are caused by stator-created harmonics. Material of the rotor core and the thickness of the core sheets are the properties to be taken into account when minimizing the rotor core losses. These losses, also known as iron losses, consist of hysteresis losses and eddy current losses. (Pyrhönen, et al, 2008)

The other part of the iron losses, hysteresis losses, are a consequence of the magnetic state changing in a steel. While the magnetic state of a steel changes along one electric cycle, the change takes place by the hysteresis loop and requires energy. The energy is proportional to the area inside the hysteresis loop and is wasted as heat. Hysteresis losses depend on the frequency f and flux density B variation. The hysteresis losses are very small because the rotor meets mainly a DC field. (Hendershot, et al, 2010)

As mentioned earlier in chapter 2, the eddy current losses depend on the frequency, material resistivity and object's external dimensions but also on the flux density. Eddy currents are a result of harmonic components that cause asynchronous field components (Hendershot, et al, 2010). These components form torque components that are trying to rotate the rotor forwards and backwards and they heat up the rotor. Also, by increasing the air gap length the iron losses of the rotor can be decreased as mentioned earlier in chapter 2.6. So, the matters that can be affected when considering this chapter's aim are steel sheet dimensions and material resistivity.

3.1 Rotor Core Material

The rotor core material can have a significant influence on the iron losses, mostly in the eddy currents, of the rotor core. To decrease the eddy current losses, high resistivity material should be utilized in the rotor. Resistivity can be increased with alloying different materials with iron. Aluminium and silicon are materials that increase the resistivity of steel considerably. So, silicon-iron and aluminium-iron are suitable compounds for rotor core material. (Pyrhönen, et al, 2008)

Rotor core lamination materials are expressed with short marking, for example M600-65A. In M600-65A, the figure "600" means that the material has iron losses, including hysteresis and eddy current losses, of 6 W/kg at a peak flux density of 1.5 T and a frequency of 50 Hz. The "65" means that the electrical sheet is 0.65 mm thick (Pyrhönen, et al, 2008). The materials that produce less losses are more expensive. So, optimum between material losses and costs must be found.

3.2 Steel Sheet Thickness

As mentioned earlier in chapter 2.4, eddy currents produce in larger monolithic surfaces more losses than in thinner sheets. Thinner lamination steels increase the length of the path for eddy currents by pushing them into the circumferential direction and the resistance R is increased (Hendershot, et al. 1994). Thus, currents in the rotor are reduced and since the

losses are of the form RI^2 the losses are decreased. Sheet thicknesses from at least 0.2 mm upwards are available (Pyrhönen, et al, 2008). Thinner materials are more expensive while producing less losses. So, again optimum between losses and costs must be found.

3.3 Flux Barriers

Rotor core sheets of large machines may have lots of holes and openings. The main objective of them is to decrease useless mass and inertia of the rotor and help in cooling (Hendershot, et al, 2010). When designing the holes in the core, one must keep in mind that these holes may not affect the machine's electromagnetic properties aimlessly. So, the flux routes should remain untouched, because any openings in the core affect the d- and q-axis inductances and thus, torque characteristics. On the other hand, holes and barriers can be used to guide the flux and to modify the machine properties. With flux barriers, for example demagnetization characteristics and torque behaviour can be changed. Flux barriers can be used for fine tuning of the machine properties.

Flux barriers have a significant effect on the reluctance torque production ability. They represent areas that are magnetically like air in the rotor core. This modifies the d- and q-axis inductances and as a result the difference between them usually changes. The change has a direct impact on the maximum reluctance torque magnitude. (Okamoto, et al, 2013)

PMs encounter a high demagnetizing field, when large currents occur for example because of a short circuit. Under large current, the armature reaction is large and demagnetization risk increases. If the operation point of the PM moves along its demagnetizing curve and goes beyond the knee point, the PM will be irreversibly demagnetized, and the performance of the machine is degraded. To prevent demagnetization, flux barriers can be added. The demagnetization risk is highest in the edges of PMs. Thus, flux barriers are usually added in the edges and they are carefully designed to achieve the best result to avoid demagnetization and spoiling the machine behaviour. While designing flux barriers, also manufacturability must be kept in mind. (Endo, et al, 2016)

4. MACHINE MODELLING AND ANALYSIS

The next phase is to create a model of each of the rotor types with different magnet configurations. Modelling is done with electromagnetic simulation software from Altair Cedrat named Flux 2D, version 2018.1. Computations are done with transient magnetic application. As a base for the model, the current design model is used. In this chapter models are analysed, and conclusions of the literary review are presented in the beginning.

Analysis that must be done for the machine are both two- and three-phase short circuit and rated load analysis. Rated load analysis is done to find out the required magnet sizes and to examine the machine behaviour at the rated load. At the rated load, torque characteristics can be evaluated and developed according to the results. Short circuit analyses are done to examine the synchronous inductance of the machine and demagnetization of the magnets. Sufficiency of pull-out torque is also examined. The worst case two-phase short-circuit takes place if the short circuit is connected at the point where the shorted phase voltages are equal. All the calculations have been performed accordingly.

4.1 Literary Review Conclusions

For the final design of the rotor magnet positioning, three different basic configurations were proposed. They can be seen in figure 2.2. For the model, that have two magnets per pole in V-position, different angles between magnets can be applied, too. The next property to variate is the magnet grade. Five different grades were proposed for the optimization process which are presented in table 2.1. Then to achieve optimal operation of the machine, magnet width, air gap length and shape are varied, skewing of the magnets is applied and slot wedges are exploited. After that, losses of the magnets may need to be decreased and this is done by utilizing segmentation of the magnets. Finally, rotor core sheet material and thickness are optimized and if needed flux barriers are utilized. Final optimization result takes into account required performance properties and total cost of the machine.

4.2 Rated Load Analyses

In this section, analyses are done with rated load models. The objective is to study the characteristics and the applicability of the different rotor types for the machine design. Torque production capability and ripple of different configurations are studied and the first plausible designs for the machine are proposed.

4.2.1 PM Thickness

From each of the magnet layouts presented in chapter 2, a FEM-model is created. The FEM-model is created for just one pole to decrease the time consumed in the computation process. At this phase, slot wedges or air gap shaping are not applied yet. All the changes in the design are done one by one and considered individually. After each modification, the voltages of the current sources must be checked to ensure that the load angle is correct. If the voltages are too small or high, a new correct load angle must be searched.

Tangentially Embedded Magnets

Figure 4.1 shows the model of the tangentially embedded magnets rotor type presented and figure 4.2 the mesh created for the model that software uses in the computation process. Figure 4.3 depicts the circuit model used in the computations at the rated torque.

Figure 4.1 Tangentially embedded magnets rotor model.

In the beginning, there were no flux barriers in the sides of magnets but after the first computations they were added to reduce PM leakage. Flux views indicated that there were high leakage fluxes in the magnet sides. The leakage fluxes decreased a lot with flux barriers and the torque with the same stator current increased.

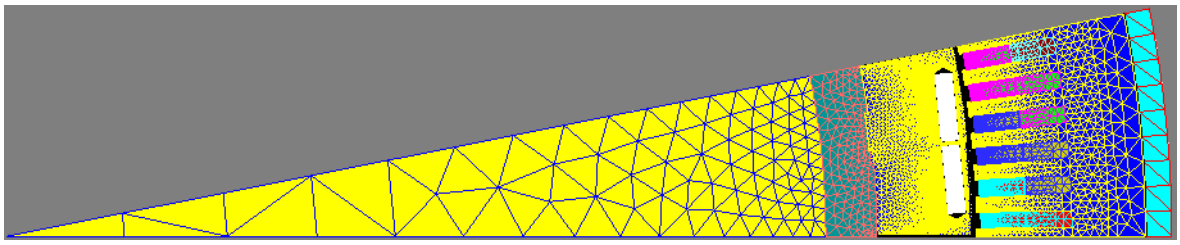

Figure 4.2 Mesh of the model.

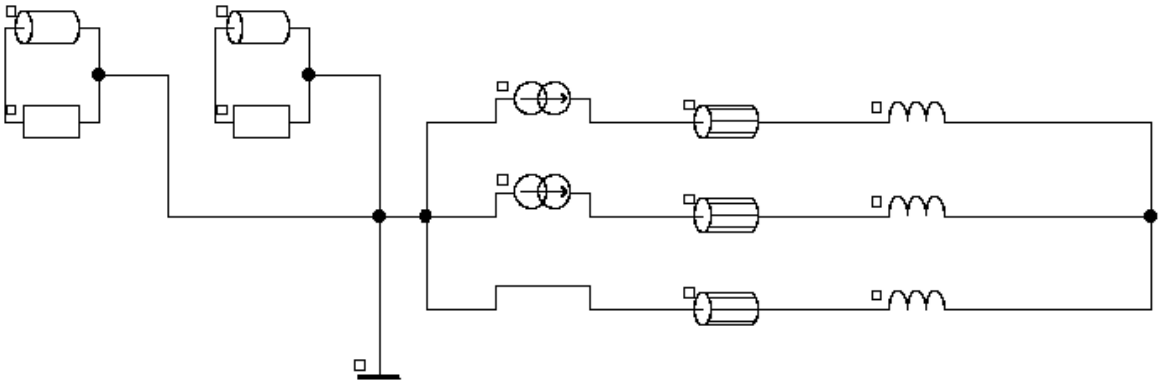

Figure 4.3 Current driven circuit model used in computations for calculating the rated torque. Circuit model has only two current sources instead of three, because Flux 2D gives sometimes erroneous results with star connected models. This approach guarantees error-free calculation of the third phase current.

At first, the magnet size needed in case of different magnet grades is found out with the help of FEA. The required magnet size is found when the rated torque 253 kNm of the current design is achieved. So, the rated load analysis is utilized. In table 4.1 the thicknesses and widths of the magnets are depicted.

Table 4.1 Magnet sizes, masses and price indices of each of the magnet grades for the tangentially embedded magnets. The reference price of the price index is the price of the grade N42TH. Price indices are based on magnet supplier's prices. Also torque ripple of each magnet thickness is included.

magnet grade	w_{PM} [mm]	h_{PM} [mm]	T [kNm]	m_{PM} [kg]	PM Price [%]	Torque ripple [%]
N42TH	68	31	252	683	100	6.46
G45UH	68	29	252	639	105	6.29
G48TH	68	25	252	551	93.0	5.74
G50UH	68	24	253	529	90.2	5.59
G52TH	68	23	253	507	82.3	5.43

The table above shows that when the remanence of the material decreases, the amount of magnetic material needed to produce the desired torque increases. The lowest price index is got with G52TH grade, so it is the most tempting choice for the final design. Later, short circuit tolerance and demagnetization is analysed and possible corrections to the grade done. The last column of the table shows the torque ripple of each of the magnet thicknesses. The maximum allowed torque ripple depends on the application. In wind power applications the maximum allowed ripple is usually below 2 % and therefore something must be done to decrease it. Torque ripple also increases when the magnet thickness increases. The reason

for this is the increased harmonic reluctance torque that causes fluctuations because of the increased saliency of the rotor.

Two Magnets per Pole in V-Position

Figure 4.4 shows the rotor model of the two magnets per pole in V-position presented. The mesh of the model is comparable with the mesh of the previous model. The angle between magnets was chosen to be 90° based on FE analyses of different angles' torque production capability with constant amount of magnet material.

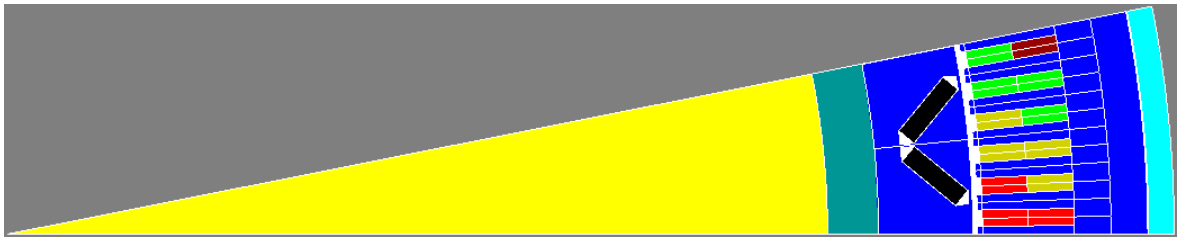

Figure 4.4 V-position rotor model.

Also, for the V-position layout flux barriers were added to decrease PM leakage fluxes. Again, the magnet sizes are found with the same principles as with tangential rotor. Results are depicted in table 4.2.

Table 4.2 Magnet sizes, masses and price indices of each of the magnet grades for the two magnets per pole in V-position. The reference price of the price index is the price of the grade N42TH from the tangentially embedded magnets rotor structure. Price indices are based on magnet supplier's prices. Also torque ripple of each magnet thickness is included.

magnet grade	w_{PM} [mm]	h_{PM} [mm]	T [kNm]	m_{PM} [kg]	PM Price [%]	Torque ripple [%]
N42TH	68	28	253	617	90.3	8.85
G45UH	68	27	252	595	97.8	8.37
G48TH	68	25	254	551	93.0	7.94
G50UH	68	24	254	529	90.2	7.59
G52TH	68	23	254	507	82.3	7.35

The table above declares the needed magnet thicknesses for each magnet grade for the two magnets per pole in V-position rotor. Price indices are also presented in the table and the reference value is the price of the N42TH grade's price for the tangentially embedded magnets rotor. So, when the magnet masses and price indices of both tangentially embedded and two magnets per pole in V-position rotors are compared, it can be said that they are very similar. The tangentially embedded magnets structure needs more magnets only with N42TH and G45UH grades. In both structures G52TH is the cheapest choice. Torque ripple is increased by about 2 percentage points with the two magnets per pole in V-position.

Radially Embedded Magnets

Figure 4.5 shows the model of the radially embedded magnets rotor in which the magnets are magnetized circumferentially. The mesh of the model used in the computations is similar with the mesh of the tangentially embedded magnets layout.

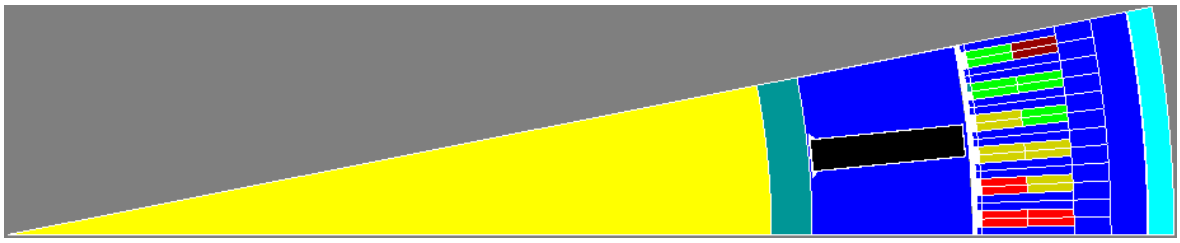

Figure 4.5 Radially embedded magnets rotor model.

For the radially embedded magnets layout, the rotor yoke must be changed to non-magnetic material to avoid short circuiting the magnet. Also, a small flux barrier was added between the magnet and rotor yoke to enforce the effect. Table 4.3 gives the magnet sizes, price indices and torque ripple of this rotor structure.

Table 4.3 Magnet sizes, masses and price indices of each of the magnet grades for the radially embedded magnets layout. The reference price of the price index is the price of the grade N42TH from the tangentially embedded magnets rotor structure. Price indices are based on magnet supplier's prices. Also torque ripple of each magnet thickness is included.

magnet grade	w_{PM} [mm]	h_{PM} [mm]	T [kNm]	m_{PM} [kg]	PM Price [%]	Torque ripple [%]
N42TH	150	31	254	753	110.3	8.67
G45UH	150	30	254	729	119.9	8.57
G48TH	150	28	254	680	114.9	8.61
G50UH	150	27	253	656	112.0	8.60
G52TH	150	26	252	632	102.6	8.65

Table 4.3 shows that the magnet mass needed for this rotor type is from 70 kg to 140 kg higher than with other magnet layouts with the same magnet grades. Also, the rotor iron mass increases, since the thickness of the rotor iron needs to be increased by 65 mm because of bigger magnet dimensions. The radially embedded magnets layout's magnets cost from 3 % to 20 % more than the tangentially embedded magnets layout with N42TH magnets. Torque ripple is about on the same magnitude as with two magnets per pole in V-position layout. As a conclusion, this rotor type is not studied any further because of its high price and increased mass.

4.2.2 PM Width

The width of PM has a significant effect on torque ripple amplitude. Effects are depicted in figure 4.3 for the tangentially embedded magnets rotor type and in figure 4.4 for the two magnets per pole in V-position rotor type. The width affects also somewhat the torque production capability.

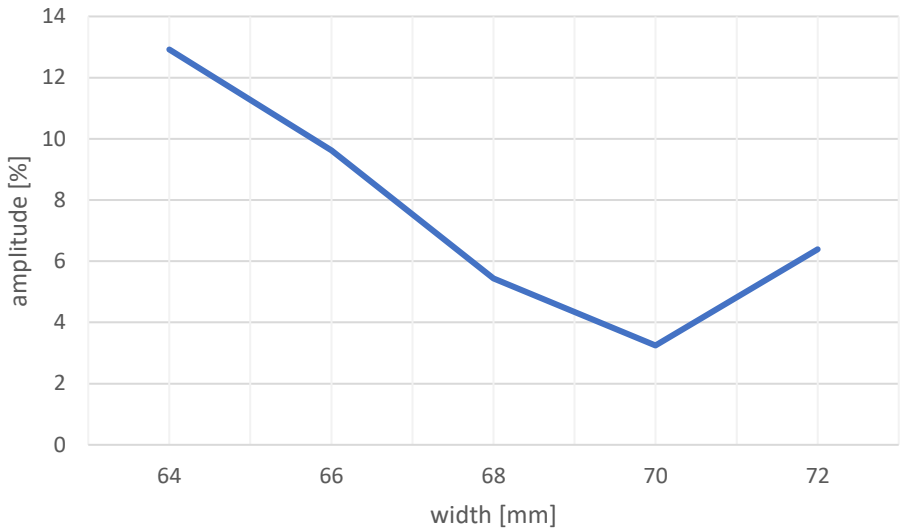

Figure 4.6 Effect of PM width on torque ripple amplitude with the tangentially embedded magnets rotor type. PM thickness is kept constant at 23 mm. The pole pitch of the machine is 186 mm. Magnet grade is G52TH, air gap length is 4.5 mm, no wedges are applied and air gap shape is uniform.

Figure 4.6 shows that the minimum torque ripple is achieved with 70 mm magnet width with the tangentially embedded magnets rotor type. Anyway, as the objective of the thesis is to minimize costs with good enough performance, at this point, the width that offers minimum costs is of great significance. The minimum cost (price index 82.3 %) is got with 68 mm wide and 23 mm thick magnet. This solution offers the second lowest torque ripple.

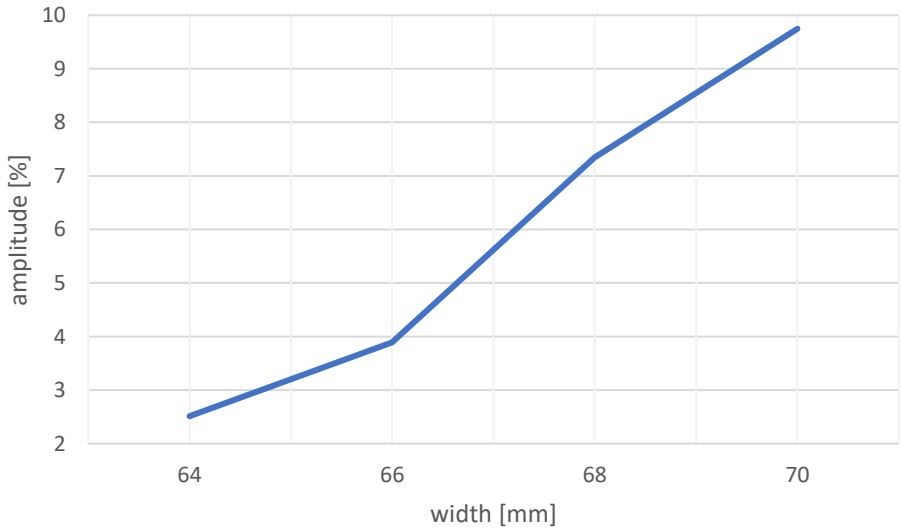

Figure 4.7 Effect of PM width on torque ripple amplitude with the two magnets per pole in V-positon rotor type. PM thickness is kept constant at 23 mm. The pole pitch of the machine is 186 mm. Magnet grade is G52TH, air gap length is 4.5 mm, no wedges are applied and air gap shape is uniform.

Figure 4.7 depicts that the torque ripple decreases as magnet width decreases. The difference between 64 mm and 70 mm torque ripples is very significant, about 7 percentage points. In any case, the minimum cost (price index 82.3 %) is got with 68 mm wide and 23 mm thick

magnets. So, the minimum cost magnet is chosen for the first machine model and if requirements are not met with it, then the magnet size is changed.

4.2.3 Slot Wedges

The torque ripple is quite high and must be decreased to achieve torque ripple limits. In this section the effects of slot wedges on torque ripple are studied. Several FE analyses are done to examine how the thickness and permeability of the slot wedges affects the torque behaviour. At first the slot wedge thickness is kept constant and the wedge permeability is varied. The effects of varying the permeability is presented in figure 4.8. After permeability analyses the wedge thickness is varied and permeability is kept constant. The results of these analyses are shown in figure 4.9. Torque ripple studies are done with the tangentially embedded magnets layout magnet grade G52TH.

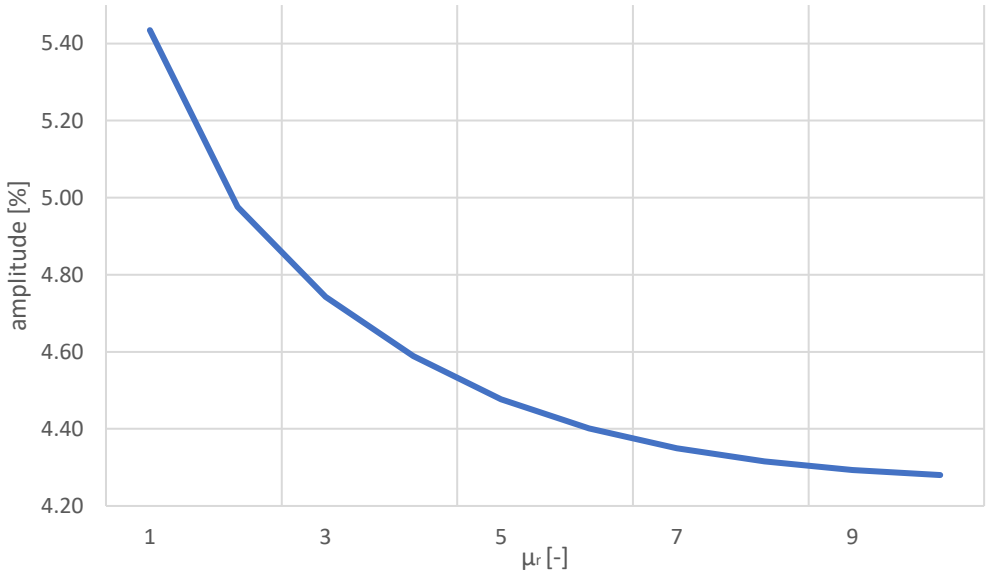

Table 4.8 The effects of slot wedge permeability on torque ripple, when the wedge thickness is kept constant at 5 mm. Tangentially embedded magnets design. Magnet grade is G52TH, air gap length is 4.5 mm and air gap shape is uniform.

Figure 4.8 depicts that torque ripple amplitude decreases by 0.7 percentage points while the relative permeability of wedges is increased from 1 to 3, so the effect is not very remarkable. After 3, the ripple amplitude decreases even slower. The produced electromagnetic torque has its maximum value (253 kNm) at $\mu_r = 3$ and after that the torque starts to decrease while the permeability of the wedges increases. This is because of increasing leakage flux on the stator side. So, semi-magnetic slot wedge, with permeability of 3, is chosen for the final design of the wedges.

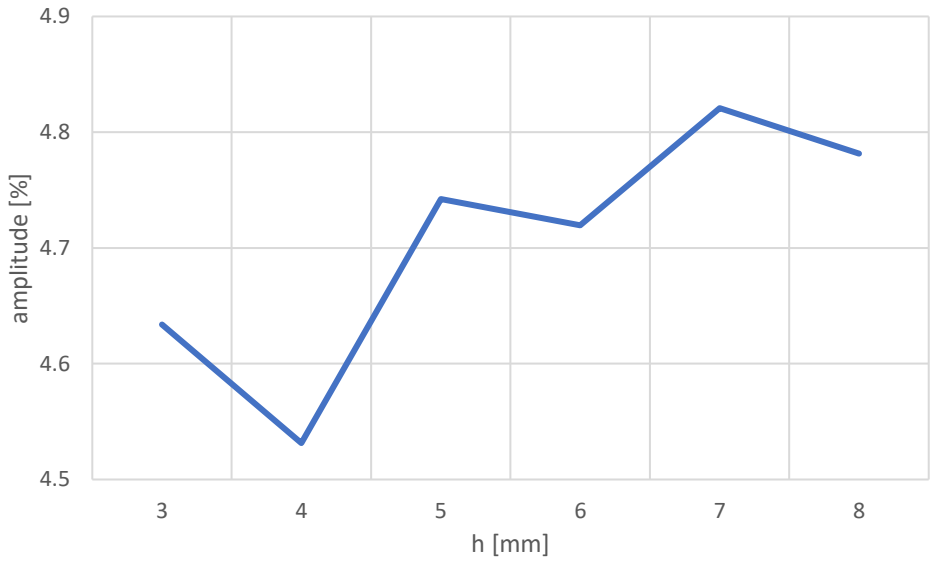

Table 4.9 The effects of slot wedge thickness h_{wedge} on torque ripple, when the wedge permeability is kept constant at ur = 3. Tangentially embedded magnets design. Magnet grade is G52TH, air gap length is 4.5 mm and air gap shape is uniform.

Figure 4.9 shows that the slot wedge thickness does not have a very significant effect on the torque ripple amplitude. The difference between the smallest and the highest ripple amplitude values is less than 0.3 percentage points. The highest torque production (253 kNm) is achieved with the 5 mm wedge. This can be explained by the fact that the main flux route permeance is also increased when a magnetic wedge is used. Thus 5 mm is chosen for the thickness of the wedges. After the proposed wedge is applied in the design, the PM eddy-current losses decreases by 12 %. Other losses stay constant.

4.2.4 Air Gap Length

The air gap length has very significant effects on the machine characteristics and losses. So, the effects of varied air gap length are studied with FEA. Figure 4.10 illustrates the effects of varied air gap length on magnet thickness and torque ripple amplitude as a function of the air gap length δ_{mech}. Figure 4.11 presents the behaviour of the price index of PMs and machine losses (iron losses and losses in magnets) as a function of the air gap length. For the loss calculation, PWM ripple of the converter with switching frequency of 2.5 kHz and amplitude of 5 % of the sinusoidal source's amplitude is added to the sinusoidal current source to make the situation more realistic from the losses point of view. Changing the air gap length affects the iron losses and losses in magnets. Study is done with the same model as in previous section and no wedges are applied.

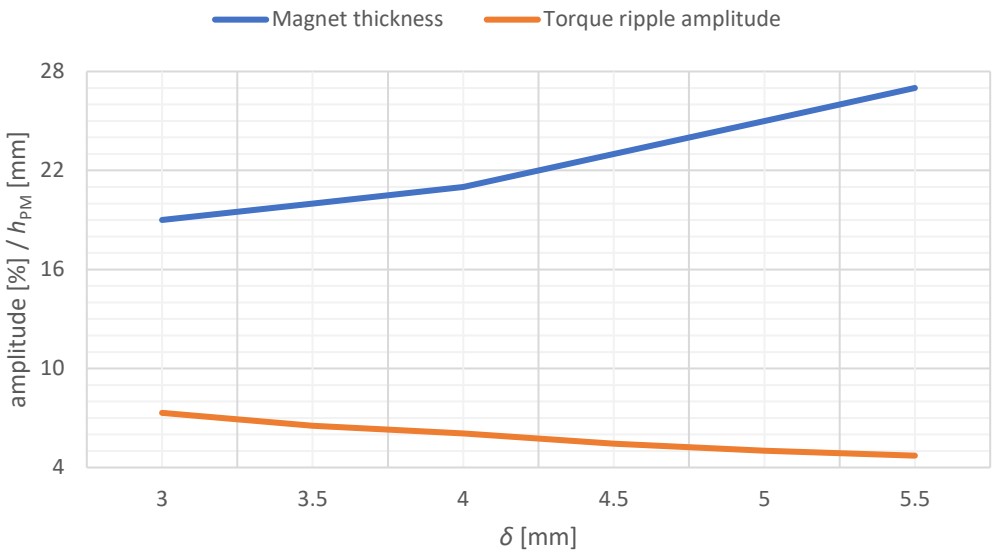

Figure 4.10 The effects of the physical air gap length δ_{mech} on the magnet height, h_{PM} and torque ripple amplitude with 68 mm wide tangentially embedded magnets. Magnet grade is G52TH and air gap shape is uniform.

Figure 4.10 shows that the torque ripple amplitude decreases quite linearly as the air gap length increases. The decrease in percentage points is about 2.6 for the whole range. The needed magnet thickness decreases, when the air gap length decreases. The decrease in the magnet height is 2 mm for every 0.5 mm decrease in the air gap length until δ_{mech} = 4 mm. With smaller values of δ_{mech}, the decrease in h_{PM} is only 1 mm.

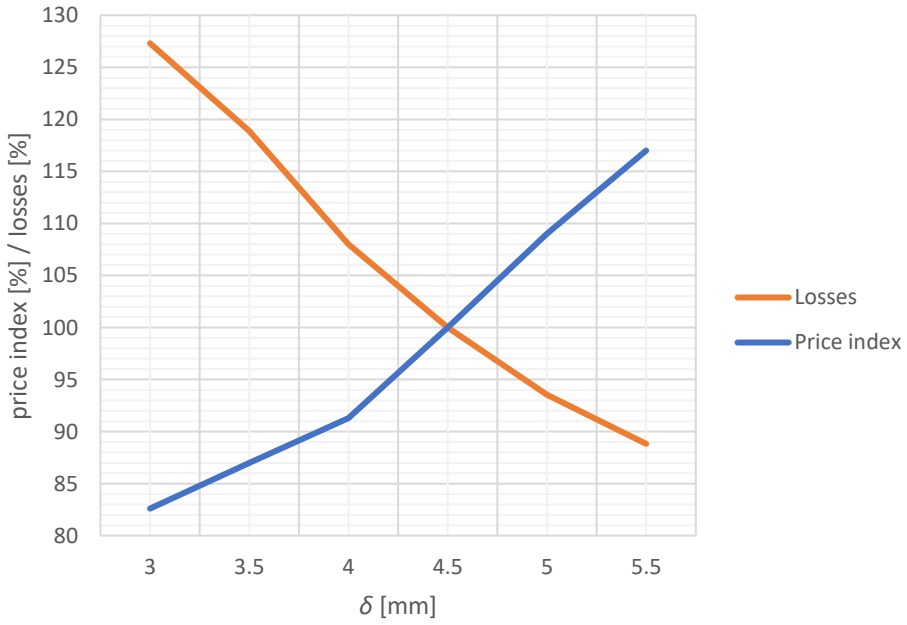

Figure 4.11 The behaviour of price index of PMs and losses as a function of air gap length with 68 mm wide tangentially embedded magnets. Magnet grade is G52TH and air gap shape is uniform.

Figure 4.11 points out that as the length of air gap increases, also the cost of magnets increases but the losses decrease. So, the optimal mechanical air gap length is where the

efficiency is high enough and cost of PMs is low enough. The minimum efficiency requirement is 97.7 % at the nominal point. At this point, the efficiency varies with different air gap lengths between 97.4 % and 97.6 %. Anyway, the air gap length is chosen to be 4 mm, since the needed PM thickness starts to decrease slower and the losses start to increase faster below δ_{mech} = 4 mm.

4.2.5 Skewing

Effects of skewing are calculated analytically for the data got from FEA. At this point only the effects on torque ripple are presented, since the effects are similar with the back-emf. Torque values with skewing applied is very simple to calculate analytically. First, the optimal skewing angle must be calculated. The angle between magnets mitigating only the slot harmonics is

$$\theta_{\text{skew}} = \frac{360°}{Q_{\text{s}}\, n_{\text{steps}}}, \tag{4.1}$$

where Q_{s} is the number of stator slots and n_{steps} the number of skewing steps. Equation (4.1) is based on idea that optimal skewing angle is a stator slot pitch. Then, the electromagnetic torque as a function of rotor angular position is needed. If optimal skewing angle is 1° with 3 steps, then the electromagnetic torque, after applying skewing, is

$$T_{\text{skew}} = \frac{T(0.0°)}{3} + \frac{T(0.5°)}{3} + \frac{T(1.0°)}{3}. \tag{4.2}$$

Figures 4.12-4.13 illustrate the electromagnetic torque ripple for both two magnets per pole in V-position and tangentially embedded magnet layouts. The figure shows the torque without skewing and with 2- and 3-step skewings. All the aforementioned methods from previous sections are applied in the models. Table 4.4 depicts the torque ripple amplitudes for both layouts and skewing models.

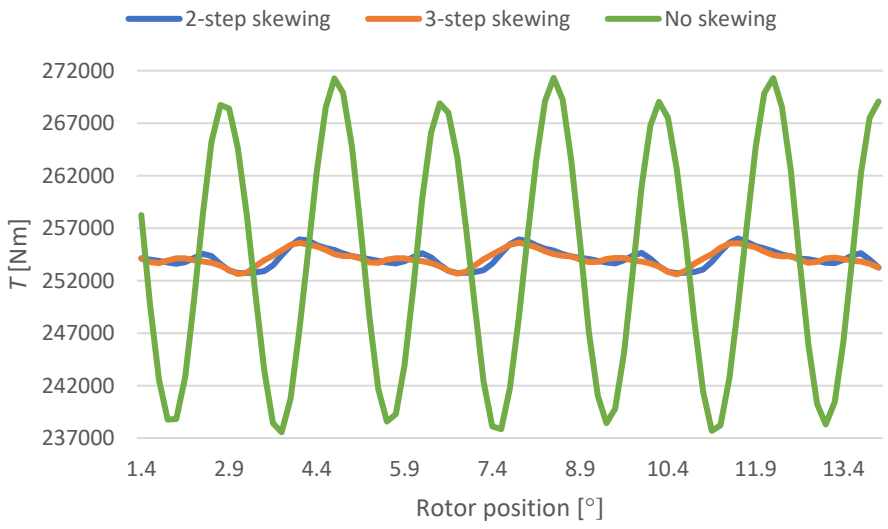

Figure 4.12 Torque ripple for two magnets per pole in V-position layout without skewing and with 2- and 3-step skewings. Magnet grade is G52TH, air gap length is 4 mm and air gap shape is uniform. PM thickness is 23 mm and it is 68 mm wide. Slot wedge thickness is 5 mm and μ_{r} = 3.

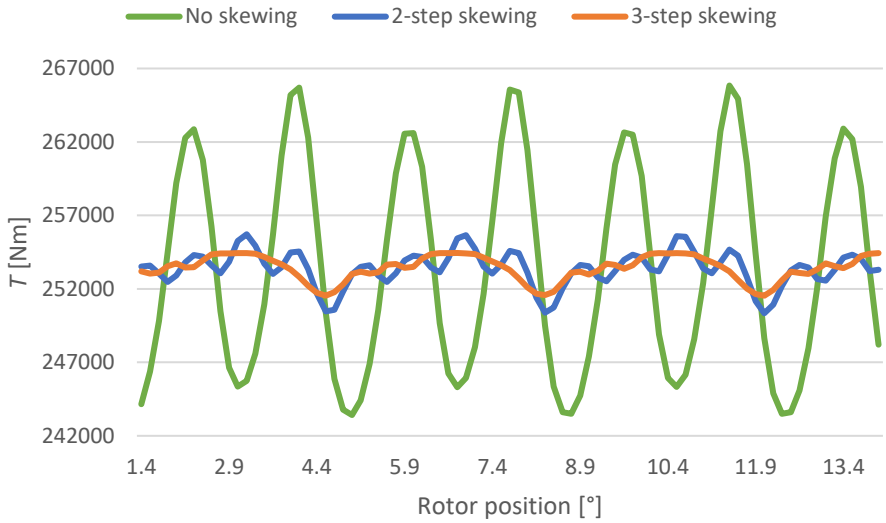

Figure 4.13 Torque ripple for tangentially embedded magnets layout without skewing and with 2- and 3-step skewings. All the properties considered in previous sections are applied, too. Magnet grade is G52TH, air gap length is 4 mm and air gap shape is uniform. PM thickness is 23 mm and it is 68 mm wide. Slot wedge thickness is 5 mm and $\mu_r = 3$.

Table 4.4 Torque ripple amplitudes for both two magnets per pole in V-position and tangentially embedded magnets layouts with and without skewings. Magnet grade is G52TH, air gap length is 4 mm and air gap shape is uniform. PM thickness is 23 mm and it is 68 mm wide. Slot wedge thickness is 5 mm and $\mu_r = 3$.

PM layout	No skewing	2-step skewing	3-step skewing
tangentially embedded magnets [%]	4.47	1.06	0.57
two magnets per pole in V-position [%]	6.71	0.65	0.60

The figures above show that the torque curves become smoother and have less pulses with the skewed rotor. From the non-skewed curves, one can calculate the number of slots in a pole pitch. As the pole pitch is 11.5 °, there are 6 peaks during a pole pitch which equals the number of slots in the stator in a pole pitch. From the table 4.4, the torque ripple amplitude without skewing for the tangentially embedded magnets design is about 4.5 % and for the two magnets per pole in V-position design about 6.7 %. They are way over the 2 % limit. After skewing is applied in the design, the amplitudes decrease remarkably. With tangentially embedded magnets layout, the amplitude with 2-step skewing is about 1.1 % and with 3-step skewing 0.57 %. The two magnets per pole in V-position design has 0.65 % amplitude with 2-step skewing and 0.60 % amplitude with 3-step skewing. So, the torque ripple amplitudes with skewing applied are very low. The ripple amplitude of the two magnets per pole in V-position layout decreases to about one tenth of the no-skewing value with only 2 skewing steps whereas tangentially embedded magnets layout needs 3 steps to achieve the ripple amplitude of about the same size. The ripple amplitudes are in acceptable level after utilizing skewing. So, the 2-step skewing can provide low enough torque ripple amplitude.

Skewing angles from 0.3 ° to a slot pitch are studied, too, if some other angle would provide a better result. However, the smallest torque ripple amplitude is achieved with the angle got

from equation (4.1) with both rotor types. The ripple increases when the angle is decreased or increased from the optimal angle.

4.2.6 Rotor Surface Shape

Rotor surface shaping is used to decrease harmonic reluctance torques. Decreasing harmonic reluctance torque decreases also the useful torque production, so the PM thickness may need to be increased to produce the torque needed. The losses decrease too as a result of a longer air gap length in the q-axis and smaller harmonic content in the air gap flux density. Air gap shaping can also be used for decreasing the leakage fluxes in the PM fringes in this case. Leakage fluxes before the air gap shaping are depicted in figure 4.14 for the tangentially embedded magnets layout and in figure 4.15 for the two magnets per pole in V-position layout.

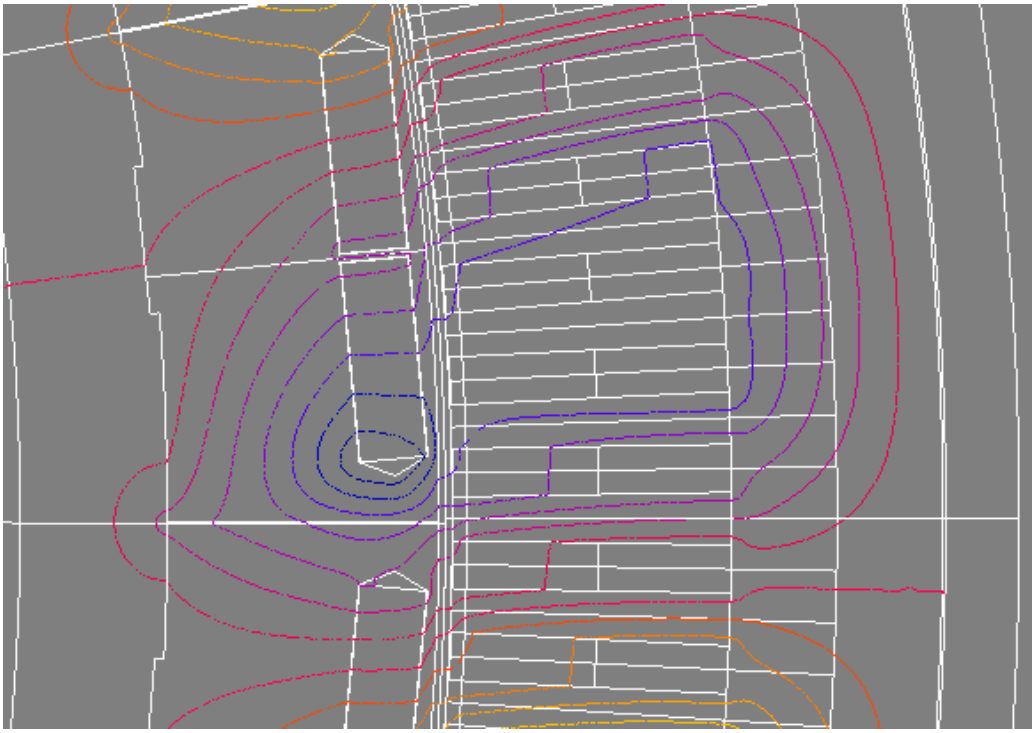

Figure 4.14 Flux plot of the tangentially embedded magnets rotor configuration. In the figure, the magnet, with the blue flux lines, has a significant leakage flux just in the fringe of the PM and only a couple of the lines cross the air gap.

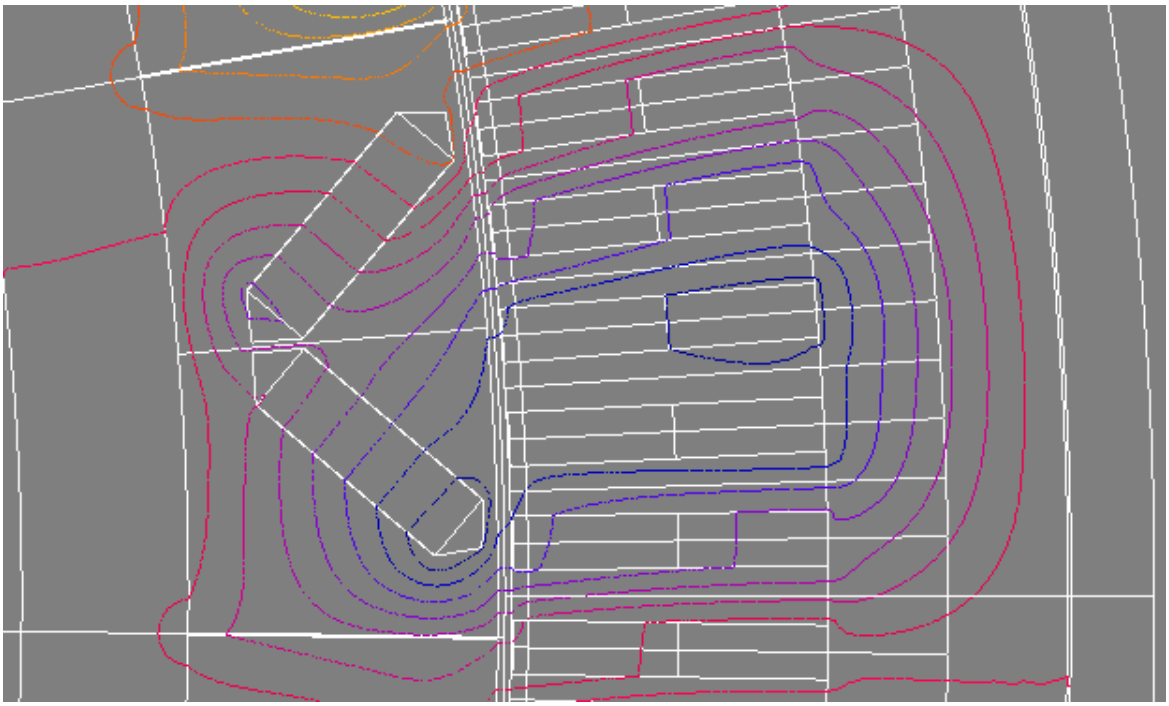

Figure 4.15 Flux plot of the two magnets per pole in V-position rotor configuration. In the figure, the magnet, with blue flux lines, has a significant leakage flux just in the fringe of the PM and only a few of the lines cross the air gap.

After several designs and computation rounds, the designs that have a high torque production capability and smooth torque curve are found for both layouts. In the new flux views (figures 4.16-4.17) one can see the new rotor models and the leakage fluxes. The needed PM thickness for both designs is 22 mm.

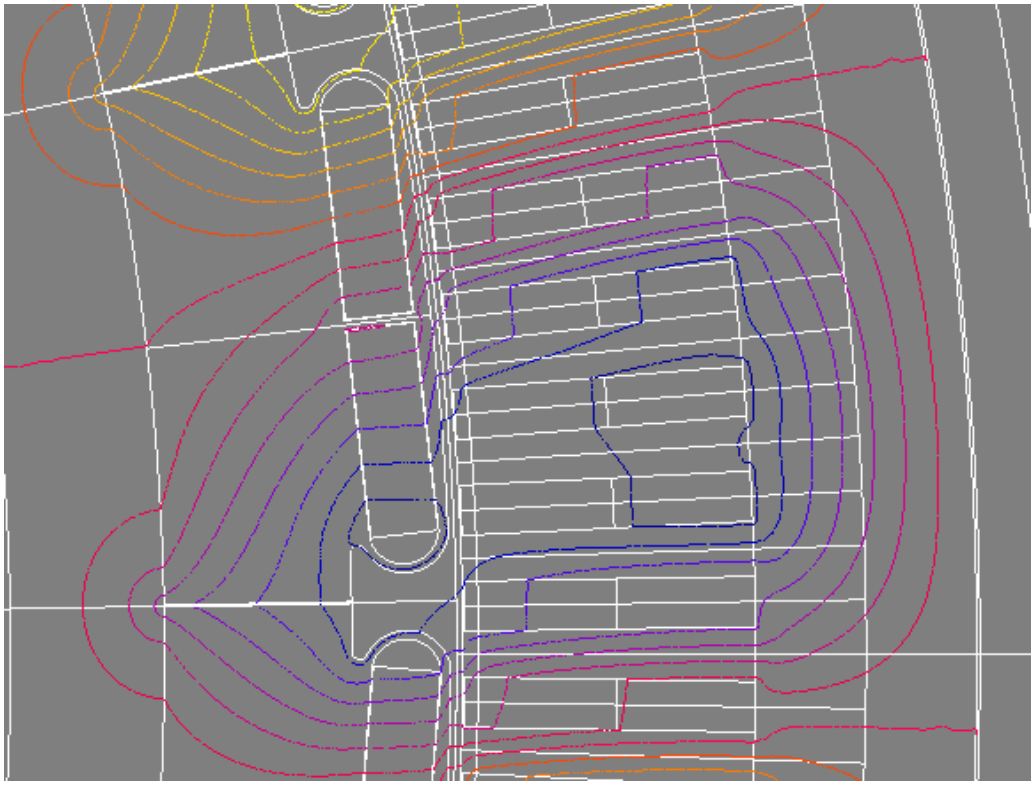

Figure 4.16 The flux view of tangentially embedded magnets layout after air gap shaping.

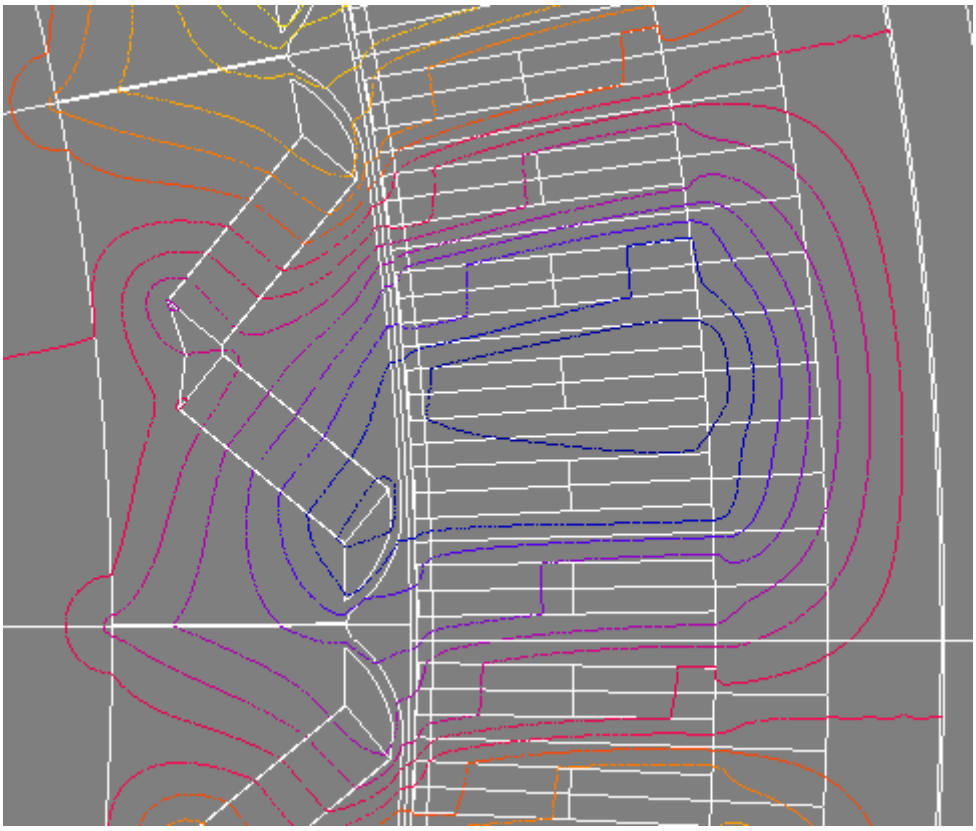

Figure 4.17 The flux view of two magnets per pole in V-position layout after the air gap shaping.

The flux views of the shaped air gap models show that the leakage fluxes of both models are decreased. Both models have equal sized magnets (w_{PM} = 68 mm, h_{PM} = 22 mm) but the shape of the air gap is somewhat different. The tangentially embedded magnets model has a longer air gap in the q-axis than the two magnets per pole in V-position model. With longer and shorter q-axis air gaps, the models produce higher ripples. The basic idea with both models is to increase the q-axis magnetic air gap length to match the d- and q-axis inductances to decrease harmonic reluctance torques.

The torque ripple amplitude values for the new designs are depicted in table 4.5. The table has ripple values with and without skewing.

Table 4.5 Torque ripple amplitudes for air gap shaped models with and without skewing.

PM layout	No skewing	2-step skewing	3-step skewing
torque ripple with tangentially embedded magnets [%]	2.89	0.87	0.81
torque ripple with two magnets per pole in V-position [%]	5.99	0.63	0.37

The table above shows that the torque ripple amplitudes without skewed rotor decreased by about 1.6 percentage points with the tangentially embedded magnets layout and about 0.7 percentage points with the two magnets per pole in V-position layout from the values before reforming the air gap. The ripple of the tangentially embedded magnet layout with the 2-step skewing decreased by about 0.2 percentage points and with the 3-step skewing increased about the same amount. With the two magnets per pole in V-position layout, the ripple stayed about the same with the 2-step skewing and decreased to 0.37 % with the 3-step skewing.

So, the 2-step skewing offers good enough results in decreasing the torque ripple below the limit in both cases. Iron losses and PM eddy current losses are now 80 % with the two magnets per pole in V-position layout and 88 % with the tangentially embedded magnets layout of the losses of the tangentially embedded magnets layout with non-shaped 4 mm air gap. Iron losses in laminations are 30 % higher with the two magnets per pole in V-position layout than with tangentially embedded magnets layout. Losses in PMs are that much higher in the tangentially embedded magnets layout.

Now, as the final designs are introduced, the full load characteristics of current and voltage can be simulated. In figures 4.18 and 4.19 are presented current and voltage waveforms for both layouts.

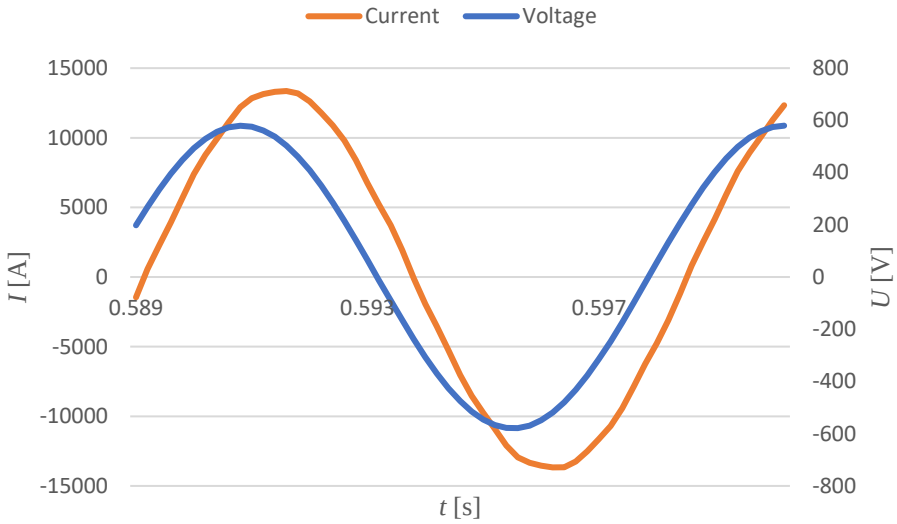

Figure 4.18 Full load current and voltage waveforms for the tangentially embedded magnets layout. The rms-value for current is 9590 A and for voltage 410 V. Power factor is 0.901.

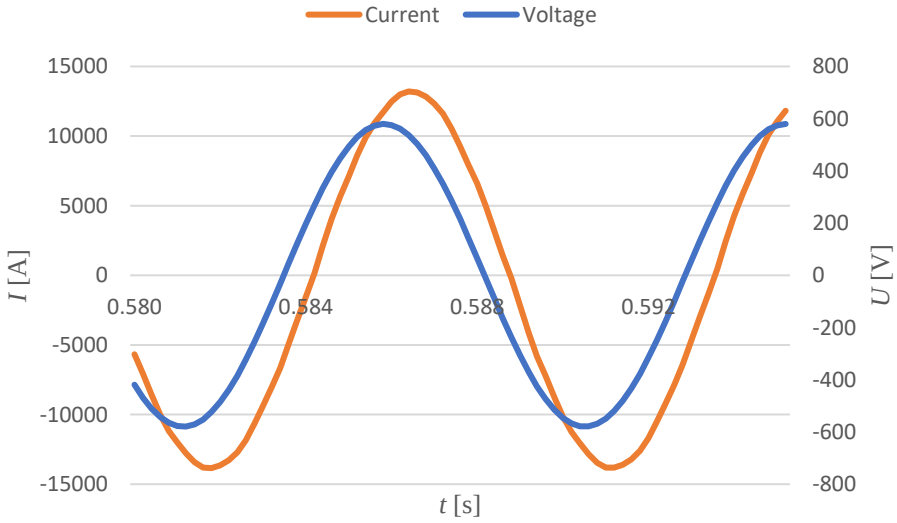

Figure 4.19 Full load current and voltage waveforms for the two magnets per pole in V-position layout. The rms-value for current is 9560 A and for voltage 410 V. Power factor is 0.906.

Figures 4.18-4.19 show the waveforms for current and voltage for both layouts. Both layouts are fed with 410 V in which case tangentially embedded magnets layout needs 9590 A and two magnets per pole in V-position layout 9560 A. Power factors are close to each other, 0.901 for tangentially embedded magnets layout and 0.906 for two magnets per pole in V-position layout.

4.2.7 Magnet Segmentation

Losses in PMs are restricted to 5.7 kW because of cooling arrangements. So, magnets must be segmented to achieve acceptable losses to avoid demagnetization. Equation for segmentation reduction factor (*SRF*) can be prove with equation (2.5). τ is chosen to be slot pitch τ_u because the aim is to suppress slot harmonics. If equation (2.5) is cancelled out with *n* the *SRF* gets the following form

$$SRF = \frac{\frac{l}{n}+\frac{\tau_u}{n}}{\frac{ml}{n}+\tau_u}. \quad (4.3)$$

In equation (4.3) $\frac{l}{n}$ means the same as the length of axial segment l_{segm}. As *m* means segments in tangential direction it equals to 1, because magnets are monolithic in the tangential direction. Then $\frac{\tau_u}{n}$ is assumed to be small in comparison with $\frac{l}{n}$ and the final form of the *SRF* is

$$SRF = \frac{l_{segm}}{l_{segm}+\tau_u}. \quad (4.3)$$

Losses of magnets in the two magnets per pole in V-position layout need to be decreased to 20 % of the original losses mentioned in the previous section. So, the magnets must be sliced to 7 mm slices. This means that *SRF* = 0.18 for the two magnets per pole in V-position layout. In the tangentially embedded magnets layout, losses in PMs must be decreased to 13 % of the solid parts losses. This means that magnets should sliced to 4 mm slices to keep the magnets fully magnetized. Then, *SRF* = 0.11 for the tangentially embedded magnets layout. So, losses in PMs are now 5.2 kW for the two magnets per pole in V-position and 4.9 kW for the tangentially embedded magnets model.

After segmentation of magnets, the efficiencies of the machines are improved. Now, efficiencies are 97.8 % for the tangentially embedded magnets layout and 97.7 % for the two magnets per pole in V-position layout. Both of the machines are now within the efficiency limit and have output power of 10.4 MW.

4.3 Pull-Out Torque

The pull-out torque is the highest torque value that the machine can produce with any load angle. The pull-out torque must typically be at least 20 % higher than the rated torque. In that case there is a reserve to deliver more power in an overloading situation and maintain synchronism. The pull-out torque of the machine is found out by changing the load angle with FEA.

At the rated voltage and speed the pull-out torque of two magnets per pole in V-position design is 348 kNm and of the tangentially embedded magnets design 375 kNm. They are 38

% and 48 % higher than the nominal torque. As a conclusion, these values are high enough and therefore no changes need to be done.

4.4 Short Circuit Analyses

Short circuit analyses are done to analyse the demagnetization of the PMs, to find out the peak- and rms-values of the short circuit current I_k and short circuit torque T_k. Both two- and three-phase short circuit analyses are done. The worst-case scenario of demagnetization takes place when the machine is operating at its rated temperature and the magnetic energy is in its maximum value when the short circuit occurs. Solving the short circuit case with FEM requires stabilized voltage-source-driven time-stepping solution with short enough time steps to maintain high resolution of the torque behaviour. From this solution phase-to-phase voltages can be evaluated. The magnetic energy is in its maximum value when one of the back-emf values is at zero in three-phase short circuit and the healthy phase back-emf is at its maximum value in two-phase short circuit. In these cases, the flux linkage has its maximum value and thus the magnetic energy has its maximum value. This causes the highest short circuit current. In the case of a three-phase short circuit, all the external voltage sources are set to zero, when the fault occurs. When the two-phase fault occurs, the healthy phase phase-voltage stays constant and the other two phases have half of the healthy phase phase-voltage and their phases are the same. To take the effect of the inertia as well as the braking torque into account, the rotor motion must be calculated applying a kinematic coupling (Aho, et al, 2017). It is also assumed that the short circuit takes place in the terminals of the machine, so no additional impedances are added in the circuit. The highest short circuit currents occur when the machine is cold. The cold and hot temperatures for the machine are 20 °C and 90 °C. The three-phase short circuit is also used to find out the synchronous inductance. Results of short circuit test are utilized in mechanical design to ensure durability, in cooling design to prevent demagnetization of PMs and in electrical design to prevent destruction of windings.

4.4.1 Two Magnets per Pole in V-Position

Figure 4.20 depicts two-phase short circuit results for the two magnets per pole in V-position layout. The figure shows the areas which will be demagnetized in the worst-case scenario when the machine is at its rated temperature. The highest demagnetizing field strength is produced in two-phase short circuit.

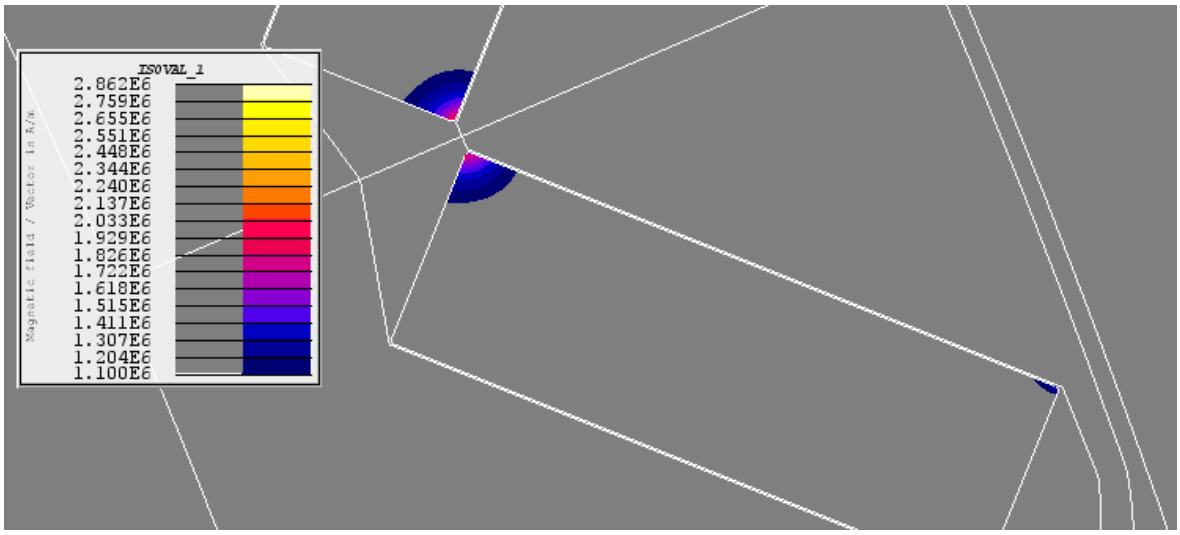

Figure 4.20 Demagnetized areas at two-phase short circuit when the machine is at its rated temperature and the short circuit takes place in the machine terminals. The figure shows the magnetic field strength values above PMs intrinsic coercivity at its rated temperature.

The figure above shows that the corners in the middle encounter very high demagnetizing field strength. The areas that are covered with some colour presented in the palette are demagnetized at 90 °C. Demagnetized area is over 2 % of the magnet volume which is unacceptable. With further iterations of the flux barrier designs, the design, in figure 4.21, is found. Only barriers, next to corners in the middle, are changed, since elsewhere demagnetized areas are insignificant and of the concern.

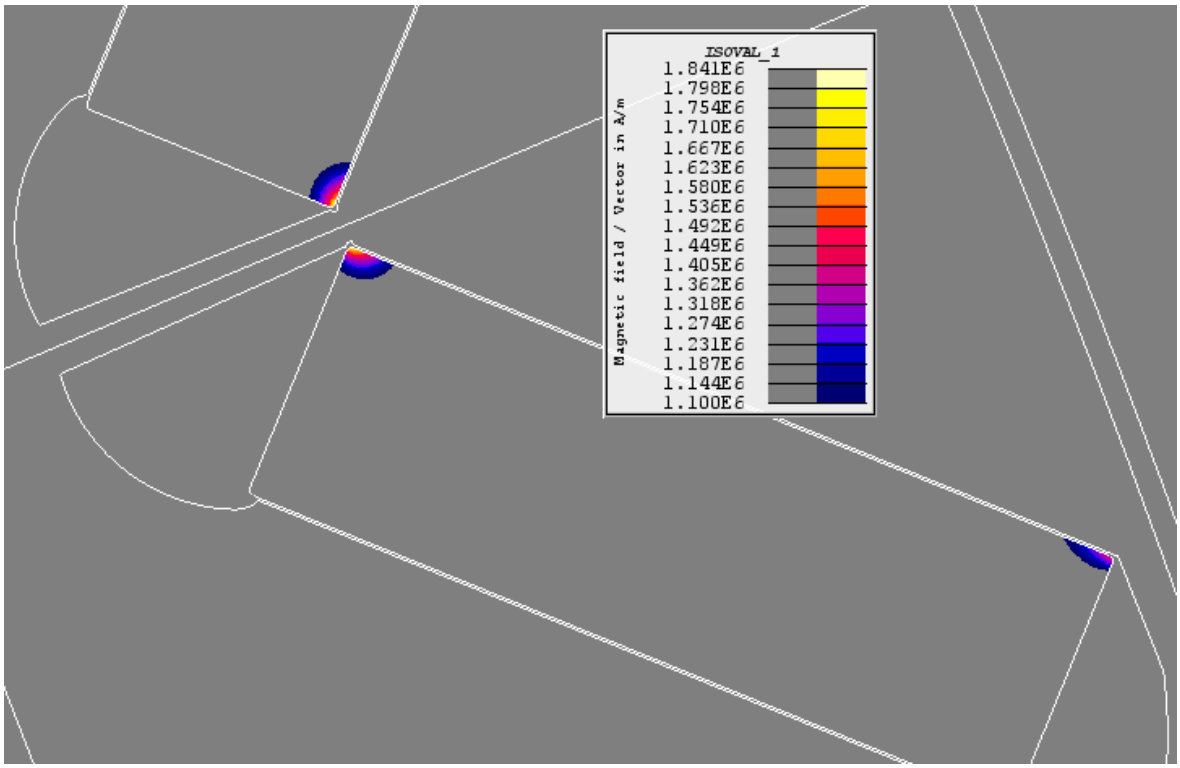

Figure 4.21 New design for the two magnets per pole in V-position layout's flux barriers to decrease the demagnetizing magnetic field strength in the PM. Demagnetized areas at two-phase short circuit are shown in the figure when the machine is at its rated temperature and the short circuit takes place in the machine terminals. The figure shows the magnetic field strength values above PMs intrinsic coercivity at its rated temperature.

New flux barrier design, seen in the figure above, decreased the magnetic field strength in the PM by about 1 MA/m and the demagnetized area is now about 1 % in the worst-case two-phase short circuit at the rated temperature. The result is still not very good, but it improved from the earlier design. Figure 4.22 depicts the magnetic field normal component for the new design in the PMs' upper surface as a function of time and PM width during the first cycle of a two-phase short circuit.

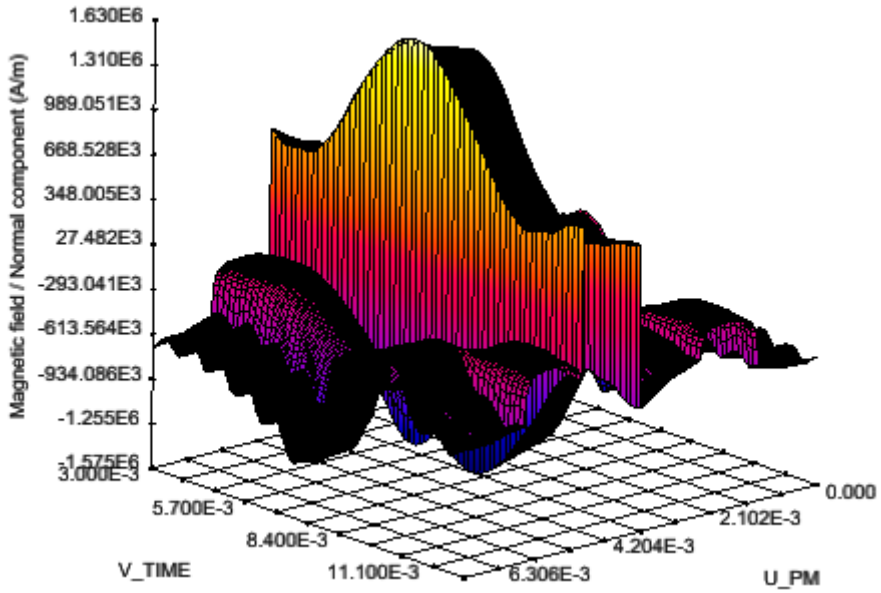

Figure 4.22 Magnetic field normal component in the PMs' upper surface as a function of time and magnet width for the two magnets per pole in V-position layout's new flux barrier design during the first cycle of a two-phase short circuit.

Figure 4.22 shows that the maximum demagnetizing field strength is 1630 kA/m. G52TH grade's intrinsic coercivity is 1830 kA/m at 20 °C. Therefore, demagnetisation may take place at temperatures higher than 39.9 °C. This is 50.1 °C below the rated operating temperature and this design should be further changed to find a better solution from the demagnetization point of view. Figure 4.23 depicts the magnetic flux density distribution and the flux lines in the rotor at a time instant when the demagnetizing field strength has its maximum value.

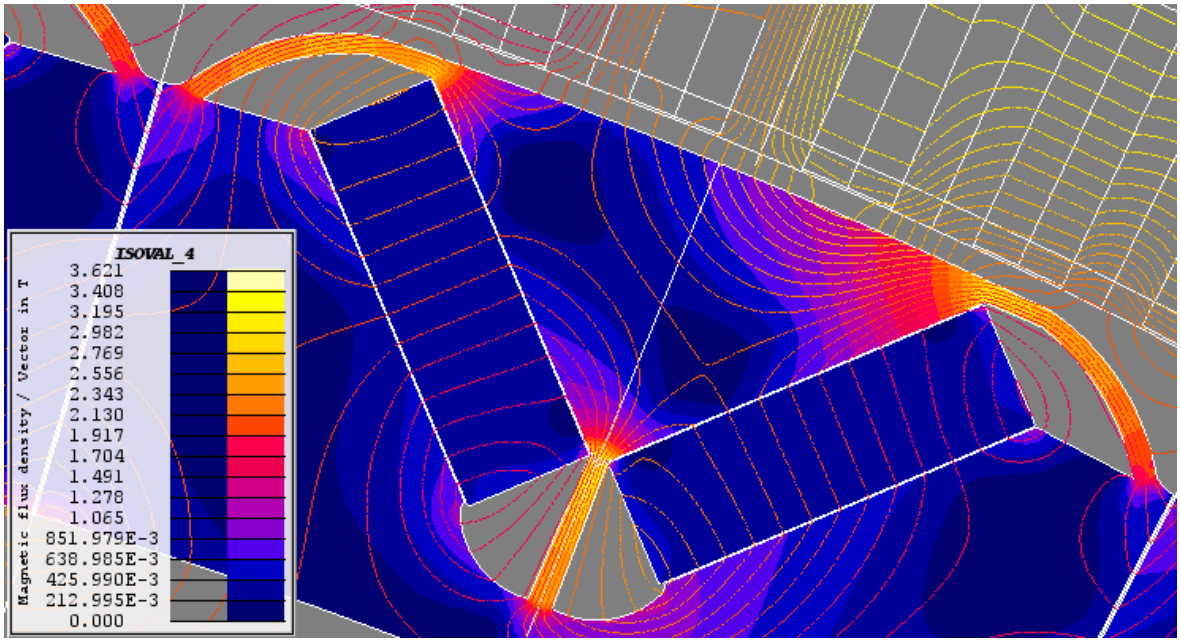

Figure 4.23 Magnetic flux density distribution and the flux lines of the two magnets per pole in V-position rotor during a two-phase short circuit at a time instant when the demagnetizing magnetic field has its highest value.

According to Kim, et al, (2009), demagnetization of the inner corners of PMs is caused by the high magnetic saturation of steel near the corners, which distorts the armature reaction flux path. Also, figure 4.23 illustrates that the rotor steel is heavily saturated. The calculation result shows that the magnetic flux density reaches values over 3 T, which may be unrealistic and the reason is explained later. In the figure it can be seen, that the flux produced by the stator, blocks the PM's flux completely inside the rotor circulating the fringes of the PMs. In other words, PMs are magnetically short circuited. In both fringes of both PMs it can be seen that the flux lines are not parallel with each other but some of the lines penetrate the side lines of the PMs. Therefore, the magnetization direction is changed in the fringes and this makes local demagnetization easier to take place. To improve the situation, the width of the narrow bridge between PMs should be increased. That would decrease the output torque and the size of PMs should be increased to produce the same torque. With this study the two magnets per pole in V-position layout was found more vulnerable to demagnetization than the tangential-magnet version. This result complies with the study made by Kim, et al, (2009).

The basic material templates of magnetic steels have *BH*-curves defined to only around 2.1 T and 100-300 kA/m in Flux 2D. Anyway, at these points $\Delta B/\Delta H$ is not yet close to the vacuum permeability. $\Delta B/\Delta H$ should approach the permeability of vacuum when the material saturates, but with aforementioned flux densities and magnetic field strengths the relative incremental permeability seems to still be in the range from 6 to 17. Physically iron saturates at about 2.0 … 2.1 T but processed electrical steels have saturation polarisation typically lower than 2 T. . Beyond this flux density any increment in flux density needs very high extra field strength. For example, getting the flux density from 2 T to 3 T an extra field strength of $1\text{T}/\mu_0$ = 796 kA/m is needed. To examine high saturation with FEM, the *BH*-curve must be extended further to even unrealistic values to find out local saturated areas. After the final defined point of the saturation curve, it is extrapolated, if higher field strengths are encountered. The *BH*-curve should be extended further, with for example with 1 MA/m beyond saturation polarization field strength, because otherwise the extrapolated values are most likely incorrect as the software extrapolates the *BH*-curve using the last slope value to extend the curve with a line. There might exist some local heavily saturated points where the field strength might reach values higher than values utilized in standard material templates leading to locally erroneous results. At these heavily saturated points the FEA results might be distorted. In this case, possibly incorrect values have a little effect on the inductance values and thus torque and current values causing inaccuracy to calculations. As a comparison, figure 4.24 illustrates the same phenomenon with the original *BH*-curve values as figure 4.23 with extended *BH*-curve values.

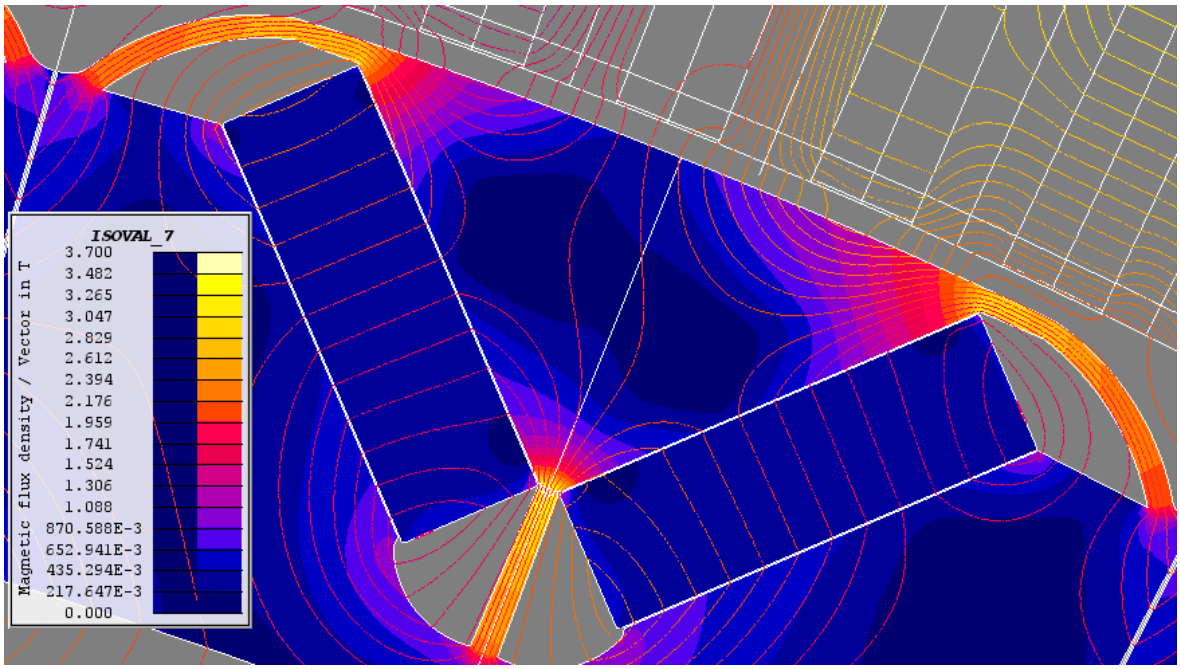

Figure 4.24 Magnetic flux density distribution and flux lines of the two magnets per pole in V-position rotor at two-phase short circuit at a time instant when the demagnetizing magnetic field has its highest value. *BH*-curve of rotor iron is directly from Flux and it is defined to 300 kA/m and 2.4 T. Beyond this point it is extrapolated.

The difference between the flux density values in figures 4.23 and 4.24 is 0.079 T which means about 2 % of the total flux density. This difference is not very large but is observable and therefore the *BH*-curve should be extended further to achieve more reliable results.

The highest torques are produced during the first cycles of a short circuit. The magnitude of torque depends also on the machine temperature. Figures 4.25-4.28 illustrate torques during two- and three-phase short circuits when the machine is at 20 °C and 90 °C.

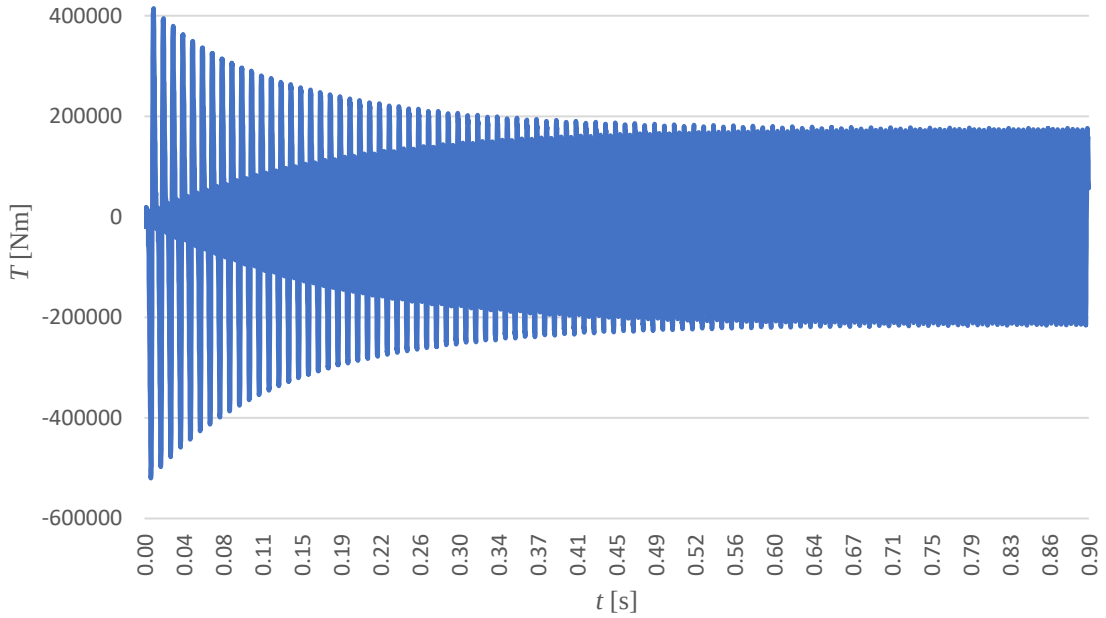

Figure 4.25 Two magnets per pole in V-position layout's two-phase short circuit torque curve as a function of time when the machine is cold (20 °C). The maximum value is 520 kNm.

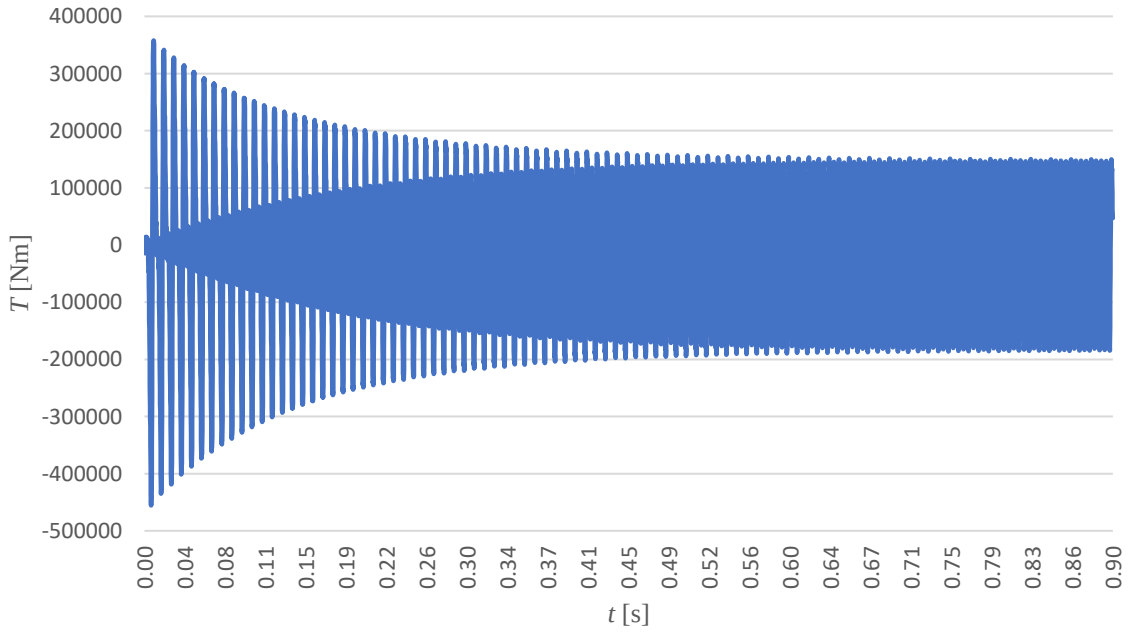

Figure 4.26 Two magnets per pole in V-position layout's two-phase short circuit torque curve as a function of time when the machine is hot (90 °C). The maximum value is 455 kNm.

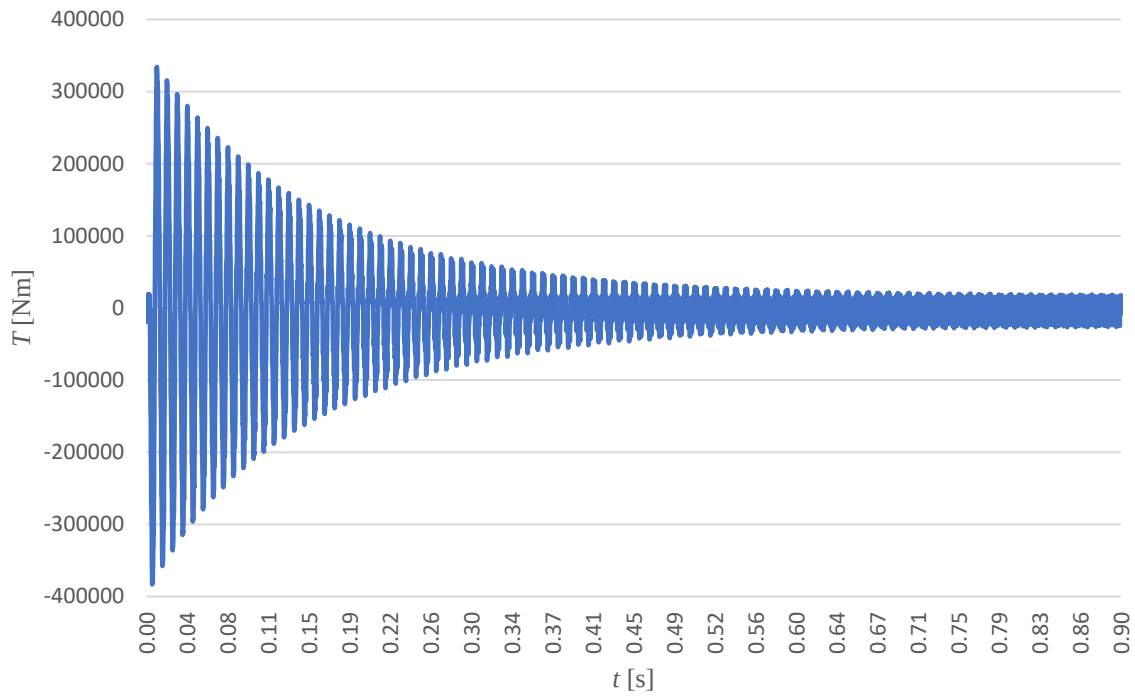

Figure 4.27 Two magnets per pole in V-position layout's three-phase short circuit torque curve as a function of time when the machine is cold (20 °C). The maximum value is 383 kNm.

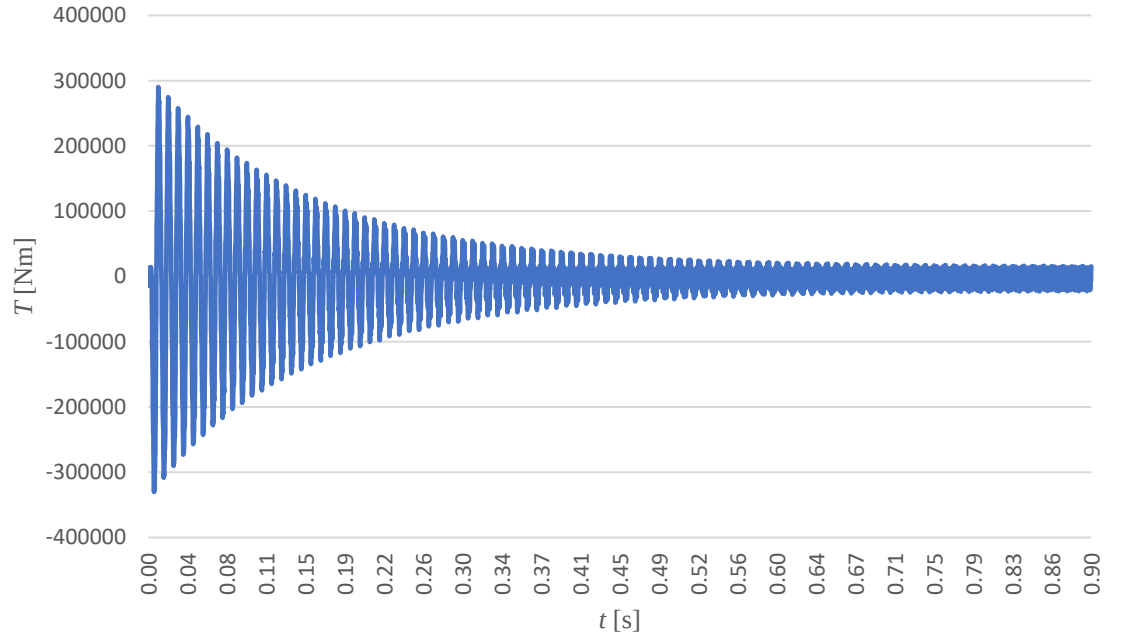

Figure 4.28 Two magnets per pole in V-position layout's three-phase short circuit torque curve as a function of time when the machine is hot (90 °C). The maximum value is 330 kNm.

Figures 4.25-4.28 indicate that the machine produces the highest torque (520 kNm) during two-phase short circuit when the machine is cold. Attenuation to steady state takes time about 0.65 s in both short circuit cases. In two-phase short circuit, the steady state level is much higher than in three phase short circuit, about 180 kNm in two-phase and about 25 kNm in three-phase short circuit. When the machine is cold, PMs have higher remanent flux

and therefore the torque is higher. In the worst-case of the three-phase short circuit, one of the back-emf values is at zero. In that case other phases have voltages that are equal but one with the positive sign and the other with the negative sign whereas in the two-phase short circuit, both faulty phases have equal voltages with same signs. So, in two-phase short circuit the sum of the stored magnetic energy is higher than in a three-phase short circuit. Thus, two-phase short circuit torque is higher. Short circuit currents are also higher because of the higher remanence when the machine is cold. Figures 4.29 and 4.30 show the short circuit currents in two- and three-phase short circuit when the machine is cold. Hot machine's three-phase short circuit current is also needed to determine the d-axis synchronous inductance and it is presented in figure 4.31.

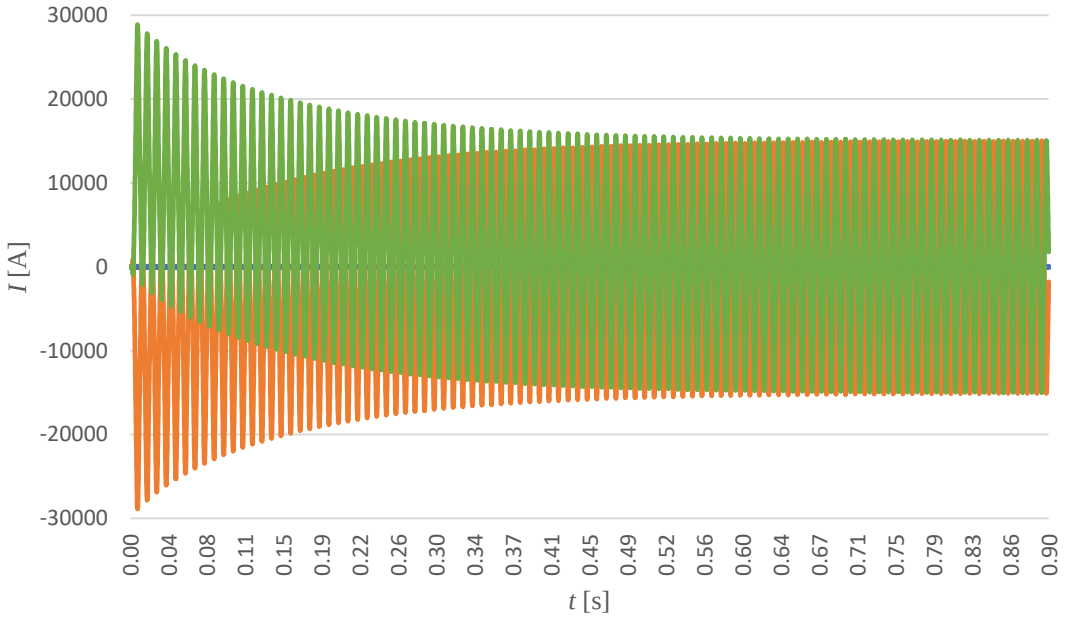

Figure 4.29 Two magnets per pole in V-position layout's two-phase short circuit current curves as a function of time when the machine is cold (20 °C). The maximum value is 28.9 kA.

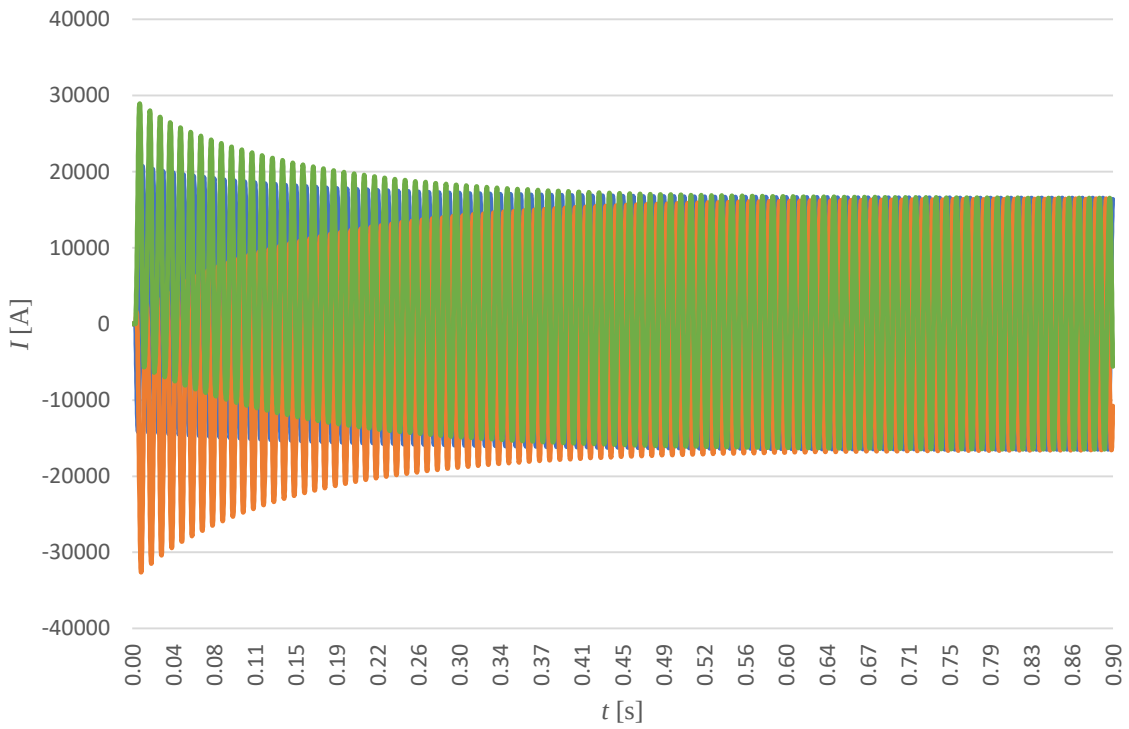

Figure 4.30 Two magnets per pole in V-position layout's three-phase short circuit current curves as a function of time when the machine is cold (20 °C). The maximum value is 32.6 kA.

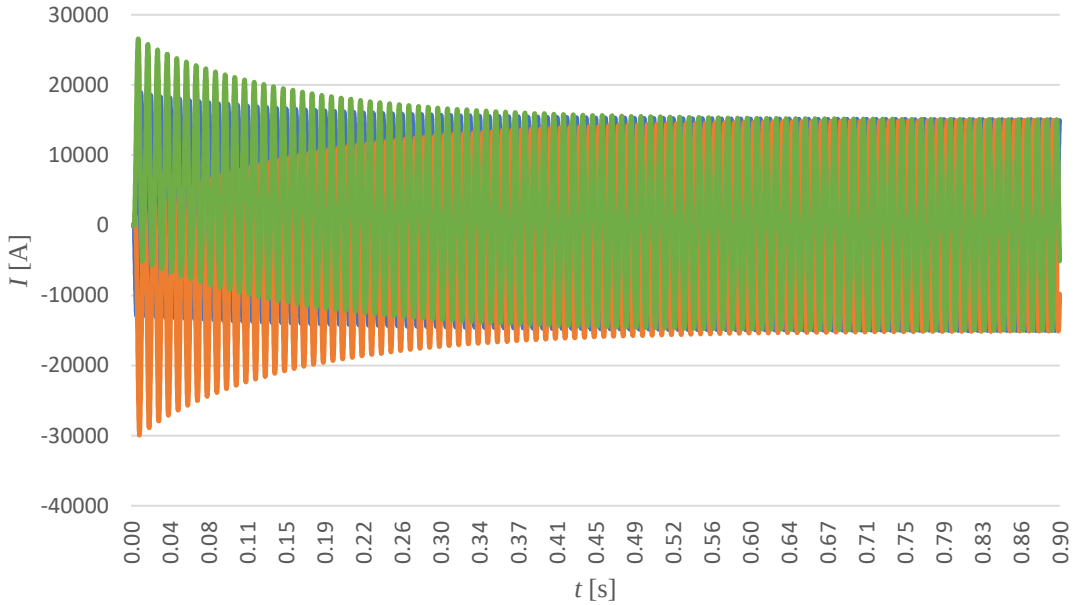

Figure 4.31 Two magnets per pole in V-position layout's three-phase short circuit current curves as a function of time when the machine is hot (90 °C). Steady state rms-value is 10.6 kA.

Figure 4.29 and 4.30 show the short circuit currents in two- and three-phase short circuits. The maximum values are about 28.9 kA in two-phase short circuit and 32.6 kA in three-phase short circuit. So, the three-phase short circuit current's peak value is 3.7 kA higher than in the two-phase short circuit whereas the torque is higher in the two-phase short circuit as was noticed earlier. Figure 4.31 illustrates the maximum value and steady state value of

three-phase short circuit currents when the machine is hot. The maximum value of the current is about 29.9 kA and the steady state rms-value is about 10.6 kA. So, the current is about 9.0 % higher when the machine is cold at three phase short circuit. The L_d can be calculated by utilizing the three-phase short circuit sustained current with equation

$$L_d = \frac{E_{PM}}{\omega_s I_k} = \frac{E_{PM}}{2\pi f_s I_k}. \quad (4.4)$$

Although, L_d cannot be calculated yet, since no load test is not done yet. No load test is needed to determine the back-emf E_{PM}.

4.4.2 Tangentially Embedded Magnets

The same short circuit tests are done for the tangentially embedded magnets layout. Figure 4.32 depicts the highest demagnetizing field strength at short circuit in the worst-case scenario when the machine is at its rated temperature. The highest demagnetizing field strength is produced at two-phase short circuit.

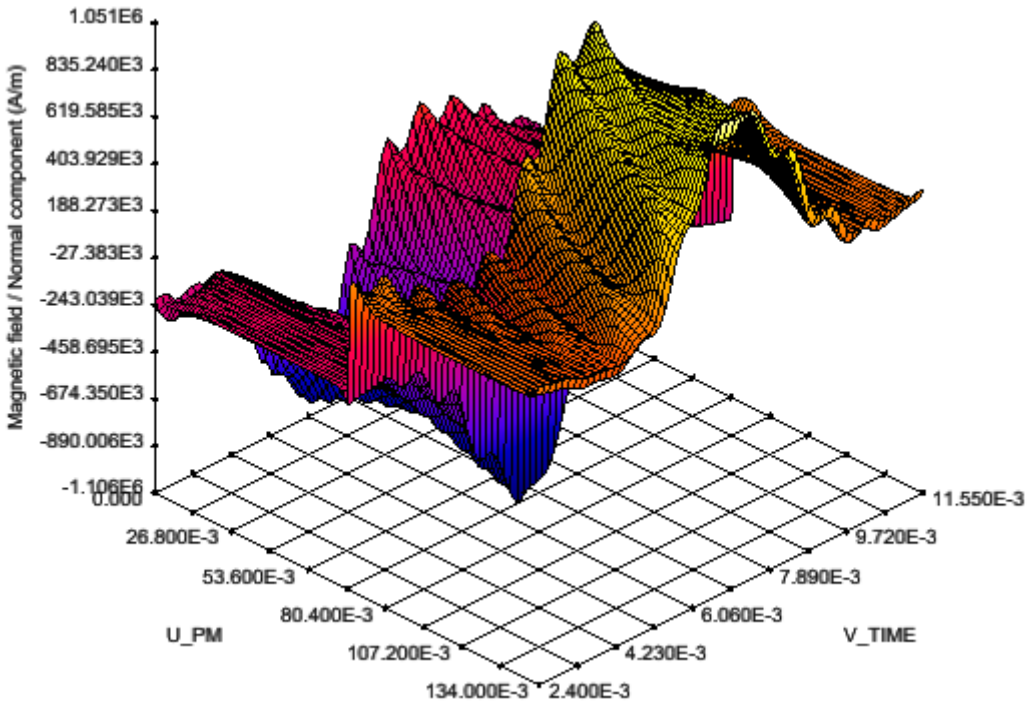

Figure 4.32 Magnetic field normal component in the PMs' upper surface as a function of time and magnet width for the tangentially embedded magnets layout during two-phase short circuit's first cycle. Worst-case scenario is utilized, and the machine is at its rated temperature (90 °C). The highest demagnetizing field strength is produced at two-phase short circuit which is 1106 kA/m.

Figure 4.32 shows that the highest demagnetizing field strength is 1106 kA/m when the machine is at its rated temperature. PM's intrinsic coercivity is 1125 kA/m at the rated temperature, so there should be no risk of demagnetization according to FEM. PM's intrinsic coercivity equals the field strength of 1106 kA/m at 91.9 °C and this is the temperature where demagnetization begins.

As it was mentioned in the previous section, the highest torque peak is during two-phase short circuit and current peak during three phase short circuit during the first cycle of short

circuit when the machine is cold (20 °C). Figure 4.33 gives the torque curve and figure 4.34 the current curves from the beginning of short circuits until sustained state.

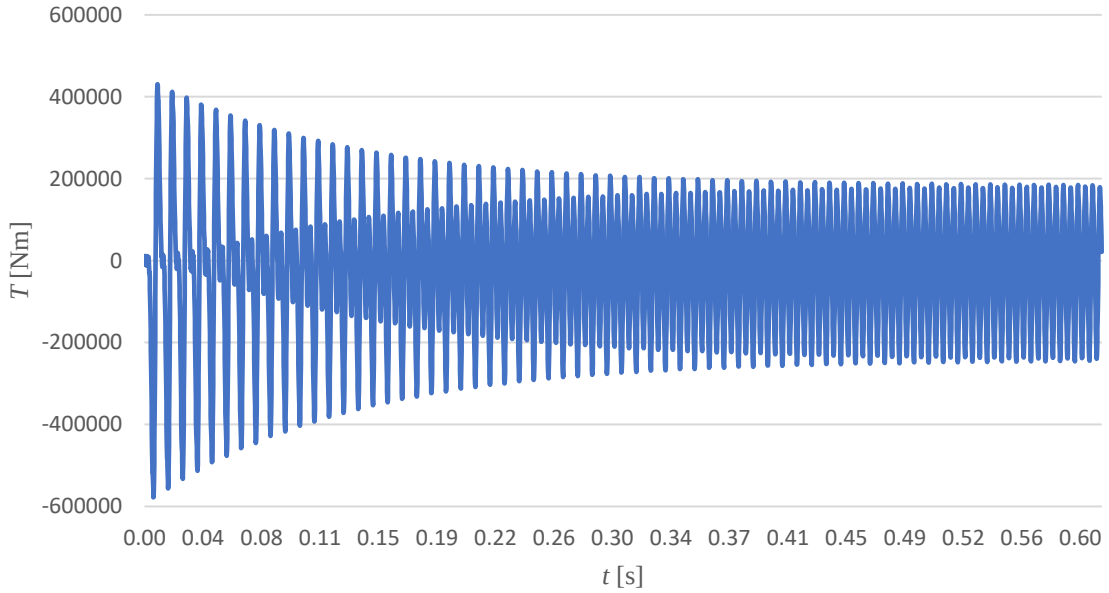

Figure 4.33 Tangentially embedded magnets layout's two-phase short circuit torque curve as a function of time when the machine is cold (20 °C). The maximum value is 578 kNm.

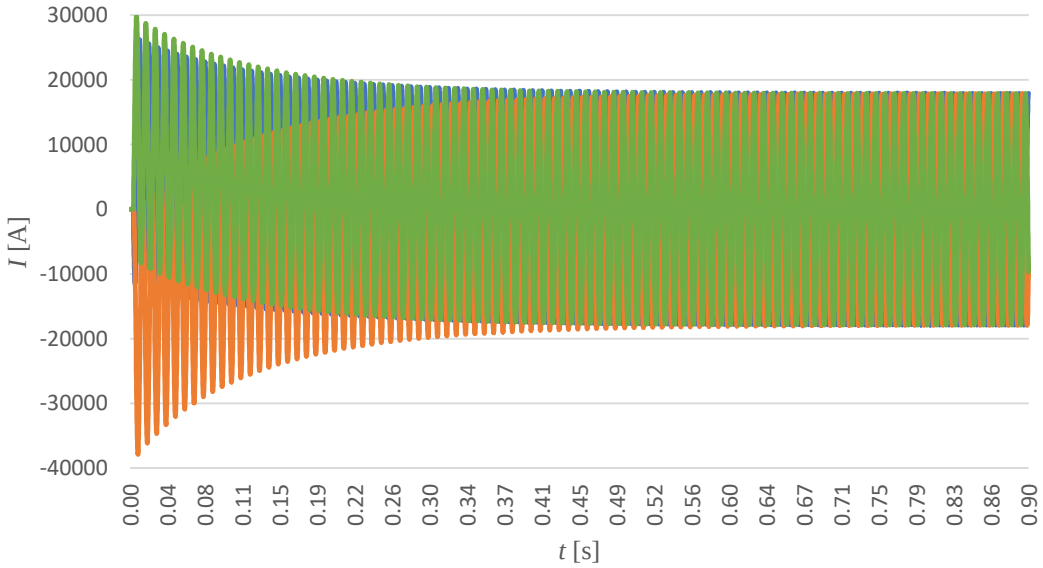

Figure 4.34 Tangentially embedded magnets layout's three-phase short circuit current curves as a function of time when the machine is cold (20 °C). The maximum value is 37.9 kA.

Figures 4.33 and 4.34 show the highest torque and current during short circuits. The highest peak value for current is 37.9 kA in three-phase short circuit and for torque 578 kNm in two-phase short circuit. Both values are on acceptable level and they are 68 kNm and 5.3 kA higher than with two magnets per pole in V-position model. Attenuation to steady state takes about 0.50 s which is 0.15 s faster than with two magnets per pole in V-position model. Figure 4.35 presents three-phase short circuit currents when the machine is at its rated temperature. Steady state rms-value of the short circuit current is needed to define L_d.

Figure 4.35 Tangentially embedded magnets layout's three-phase short circuit current curves as a function of time when the machine is hot (90 °C). Steady state rms-value is 11.5 kA.

From the short circuit test presented in the figure above, the steady state rms-value of current is 11.5 kA. This current is 0.9 kA higher than with two magnets per pole in V-position layout. So, at this point can be guessed that the tangentially embedded magnets layout has a lower L_d as it has a higher short circuit current, higher pull-out torque and faster attenuation to steady state. Attenuation is described with time constant *L/R*.

4.5 Operational Data

Operational data of both layouts from previous sections are gathered in table 4.6.

Table 4.6 Operational data of tangentially embedded magnets and two magnets per pole in V-position rotor generators from previous sections.

		tangentially embedded magnets	two magnets per pole in V-position
nominal power	P_N [MW]	10.4	10.4
nominal torque	T_N [kNm]	254	254
nominal phase-voltage	U_N [V]	410	410
nominal current	I_N [kA]	9.59	9.56
nominal power factor	cos(φ) [-]	0.901	0.906
nominal efficiency	η [%]	97.8	97.7
torque ripple at nominal torque	T_{ripple} [%]	0.87	0.63
pull-out torque	T_{MAX} [kNm]	375	348
continuous three-phase short circuit current	I_k [kA]	11.5	10.6
maximum short circuit torque	$T_{k,MAX}$ [kNm]	578	520
PM size	PM size [mm^3]	22×68×4	22×68×7
demagnetization temperature	T_{demag} [°C]	91.9	39.9

Table 4.6 shows that both machines have the required 10.4 MW power, 254 kNm torque and 410 V supply voltage. The two magnets per pole in V-position layout has slightly lower current and torque ripple but a little higher power factor than the tangentially embedded magnets layout. The tangentially embedded magnets layout has 0.1 percentage points higher efficiency and 27 kNm higher pull-out torque. Both properties are favourable from the operational point of view. As a conclusion from the table above it can be said that both of the machines would fulfil all the requirements in normal operating conditions. However, during a short circuit the difference is significant. The two magnets per pole in V-position layout is easy to demagnetize during a short circuit and therefore it has to be abandoned. Demagnetization starts already at 39.9 °C whereas with tangentially embedded magnets layout it starts above the rated temperature at 91.9 °C. The lower efficiency and pull-out torque are not desirable properties either. Because of aforementioned reasons study is continued only with the tangentially embedded magnets layout.

4.6 No Load Analysis

No load test is done to determine the magnitude of back-emf for calculating the L_d and usually back-emf value is either limited by converter dc-link maximum voltage or dc-link is designed according to generators maximum back-emf. No load test is also utilized in determining the torque ripple of the machine at that condition, which is also known as cogging. Tangentially embedded magnets layout's no load back-emf waveform is presented in figure 4.36 and torque in figure 4.37.

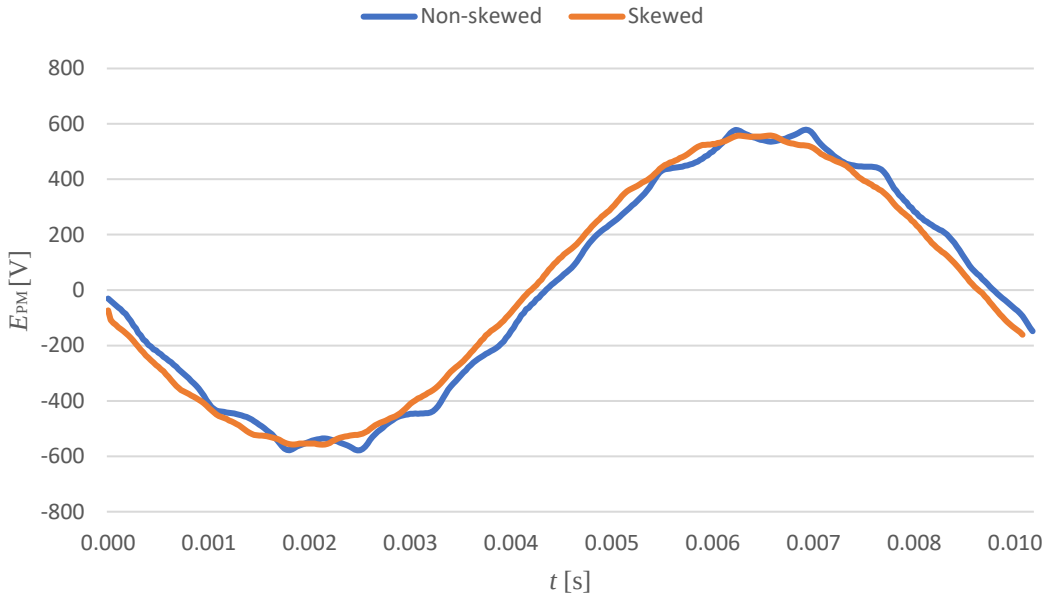

Figure 4.36 Back-emf waveform at no load for the tangentially embedded magnets layout with and without skewing (two-step). Rms-value for skewed rotor is 394 V. Skewing decreases voltage by about 2 V.

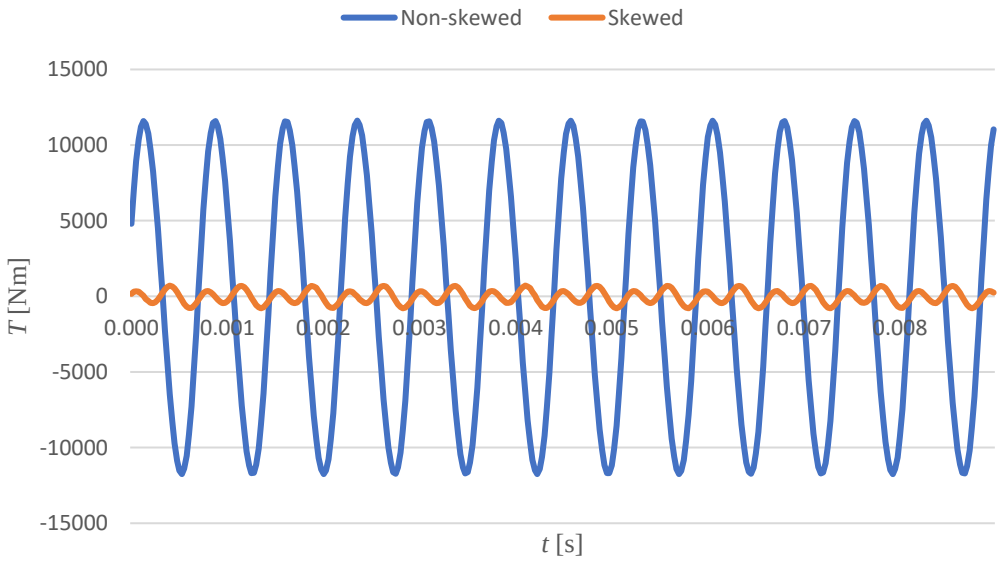

Figure 4.37 No load torque for the tangentially embedded magnets layout with and without skewing. Torque ripple is 4.6 % of the nominal torque without skewing and 0.29 % with skewing.

Figure 4.36 shows that the back-emf waveform was smoothened remarkably with the applied two-step skewing and the back-emf rms-value is 394 V and it decreased by about 2 V from the non-skewed value. Figure 4.37 shows that torque ripple at no load is 4.6 % of the nominal torque without skewing and 0.29 % with skewing. So, the torque is also smoothened remarkably after applying skewing. For calculating the inductances, no-load test is also done for the two magnets per pole in V-position layout. Thus, no load back-emf for the two magnets per pole in V-position model is 392 V.

Figures 4.38 and 4.39 depict the air gap flux density waveform and its harmonic components. Harmonic components are interesting because they cause fluctuations in the air gap flux density waveform and cause losses.

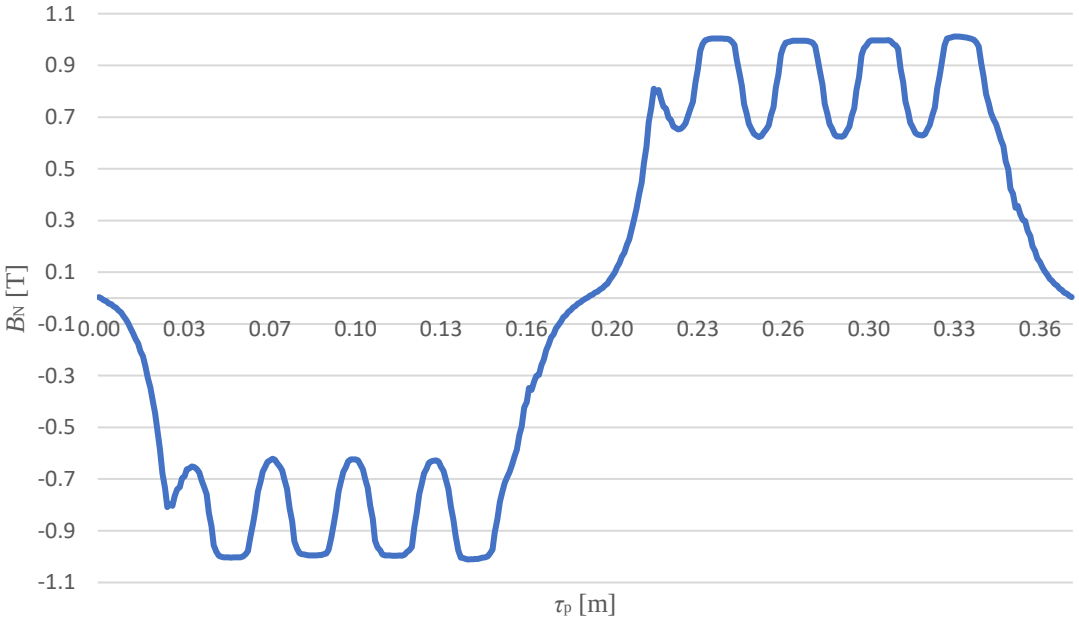

Figure 4.38 Air gap flux density normal component waveform at no load as a function of pole pitch.

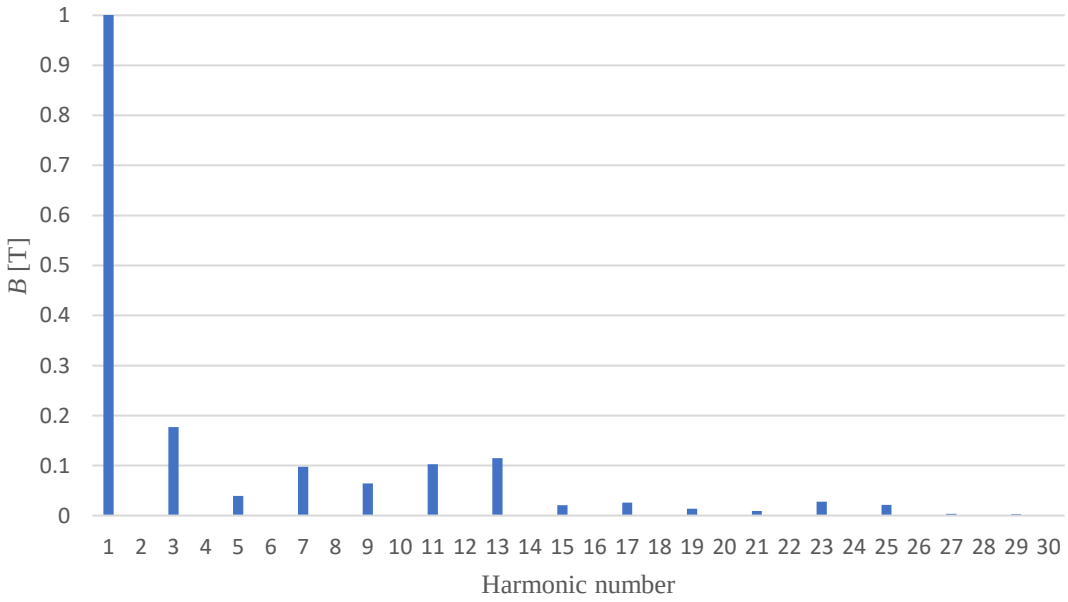

Figure 4.39 Air gap flux density normal component's harmonic components. Fundamental component is 1.01 T, 3rd 0.177 T, 7th 0.097 T, 9th 0.064 T, 11th 0.103 T and 13th 0.115 T.

Figure 4.38 shows that air gap flux density waveform is trapezoidal. From the waveform one can see slotting effect but the effects of low order harmonic components cannot be seen very clearly. Some small abrupt dips can be seen in the waveform and they are in the place where couple of low order harmonic components are in the same phase against the fundamental

component and the second peak is lower than the ones next to it because harmonic components' peaks are in opposite phase with the fundamental. Figure 4.39 shows the amplitudes of each harmonic components. The fundamental component is 1.01 T. 3rd, 7th, 11th and 13th are the highest components after the fundamental. Usually the 3rd harmonic is not visible in the current waveform of a three-phase machine because phases compensate each other's 3rd harmonic component (Pyrhönen, et al, 2008).

4.7 Synchronous Inductance

Now, as the back-emf values 394 V for the tangentially embedded magnets layout and 392 V for the two magnets per pole in V-position layout were found out in the previous section, the synchronous inductance L_d can be calculated with equation (4.4). Sustained short-circuit current is 11.5 kA for the tangentially embedded magnets layout and 10.6 kA for the two magnets per pole in V-position layout. The frequency is 106.7 Hz, respectively. With these values L_d = 0.051 mH for the tangentially embedded magnets model and L_d = 0.055 mH for the two magnets per pole in V-position model. To determine L_q, solving application in Flux must be changed to steady state magnetic solving. The machine's stator is supplied with nominal voltage and rotor excitation is removed by replacing PMs with air. Then as the rotor rotates with a slip, the machine's rms-value of current varies as a function of rotor position. The rms-values of currents as a function of rotor position are presented in figures 4.40 and 4.41.

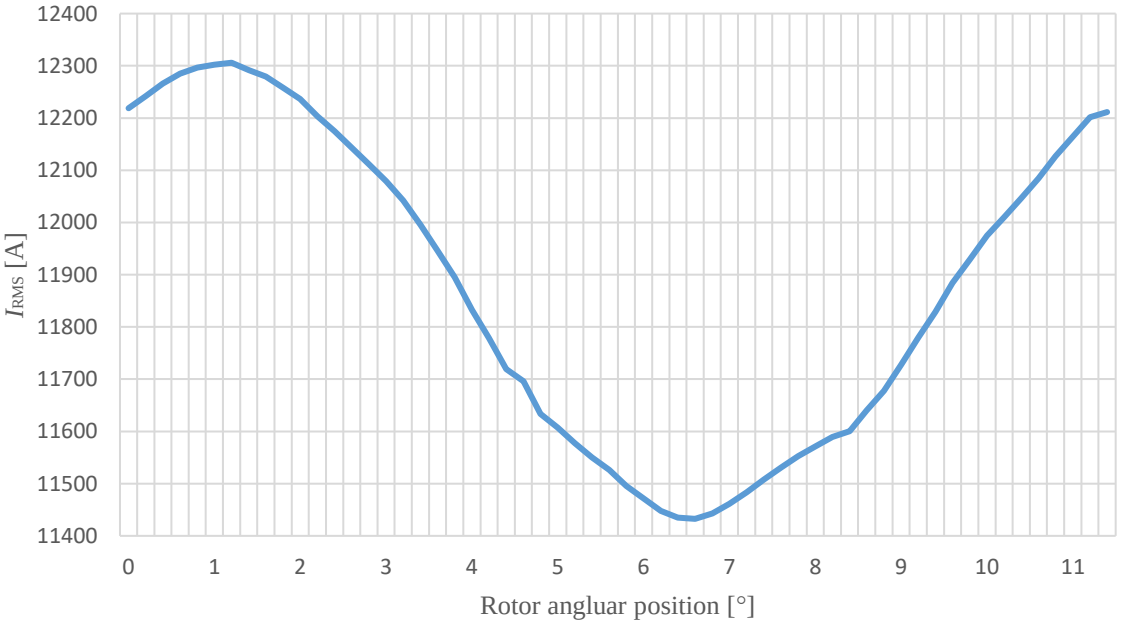

Figure 4.40 Tangentially embedded magnets layout's rms-value of current as a function of rotor position when the machine is stator magnetized and the rotor magnetization is removed, and the rotor has been running with a slip to find L_d and L_q. The figure shows the current of one electrical slip period which in total accounts for 11.25° with 32 pole machine. The maximum and minimum values of the stator current are 12.3 kA and 11.4 kA.

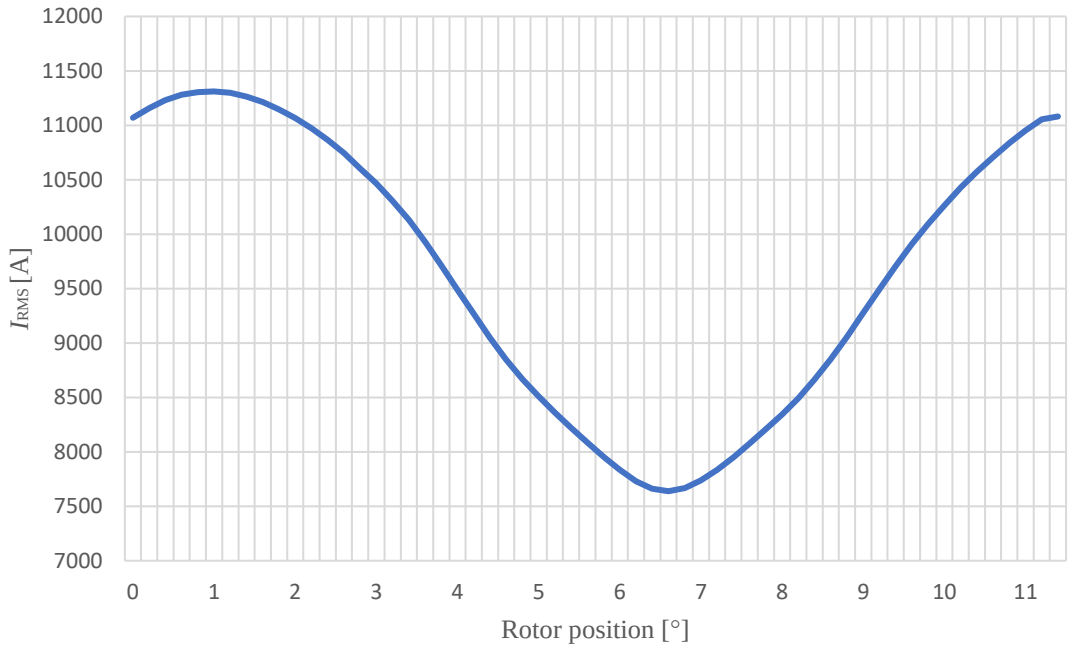

Figure 4.41 Two magnets per pole in V-position layout's rms-value of current as a function of rotor position when the machine is stator magnetized and rotor magnetization is removed, and the rotor is running with a slip. The figure shows the current of one electrical period which is 11.25° with 32 pole machine. Maximum and minimum values of current are 11.3 kA and 7.64 kA.

Figure 4.40 shows that with the tangentially embedded magnets layout the maximum value of current is 12.3 kA and minimum value is 11.4 kA. The machine is therefore slightly salient and has different currents on the d- and q-axis. Embedded PM machines are almost without exception inversely salient, so the d-axis inductance is lower than the q-axis inductance. Therefore, the d-axis current is higher than q-axis current. The d-axis is located where current has its maximum RMS value and q-axis where the current has its minimum RMS value. Angular difference between the d- and q-axis should be 90 in electrical degrees. So, with a 32 pole machine the angle is 5.63°. In the figure, the angle between the minimum and the maximum value is about 5.3°, so it corresponds with the theory. The maximum value is about 8 % higher than the minimum value, so L_q is 8 % higher than L_d. Thus, L_q = 0.055 mH. Now, as the inductances are known, the load angle can be calculated with equation (1.5) and it is 51.8° and the share of reluctance torque of the total torque is 5.0 %.

Figure 4.41 shows that with the two magnets per pole in V-position layout the maximum value of current is 11.3 kA and minimum value is 7.64 kA. The angular difference between these values is about 5.6° so it is close to the theoretical angle. The ratio between the maximum and the minimum current is 1.48 and thus, L_q = 0.082 mH. So, this model is more salient producing also more reluctance torque than the tangentially embedded magnets layout. The load angle of this model at the nominal point is 68.6° and the share of the reluctance torque of the total torque is 20.9 %. Inductance and torque values for both tangentially embedded magnets and two magnets per pole in V-position layouts are depicted in table 4.7.

Table 4.7 Comparison of inductances, load angels and torque production of both rotor constructions.

	tangentially embedded magnets	two magnets per pole in V-position
L_d [mH]	0.051	0.055
L_q [mH]	0.055	0.082
δ [°]	51.8	68.6
T_{tot} [kNm]	254	254
T_{rel} [kNm]	-12.8	-53.0
T_{PM} [kNm]	267	307

4.8 Rotor Laminations

Rotor laminations do not cover a significant amount of total losses because of the DC-flux in the rotor. Loss in the rotor core laminations for 0.5 mm sheet, which is used in the first loss calculation, is 0.54 % of the total losses. Table 4.8 lists the iron losses in the rotor laminations with different sheet thicknesses. Sheet thicknesses used in the study are commonly used thicknesses in the machine design. The results are compared to 0.5 mm lamination sheet's loss.

Table 4.8 Normalized rotor iron losses and efficiency of the tangentially embedded magnets rotor model with different lamination sheet thicknesses. The reference value is the loss with M800-50A sheet.

lamination thickness [mm]	1	0.65	0.5	0.35
normalized iron losses [%]	350	162.5	100	52.5
efficiency [%]	97.79	97.81	97.82	97.82

In table 4.8 it can be seen that the effect of the rotor lamination sheet thickness on the total efficiency of the machine is insignificant. The effect in efficiency can be seen in the second decimal, so from that point of view it does not matter whether to choose thick or thin sheets. If one compares the change in iron losses, it can be seen that losses increase quite linearly from 0.35 mm sheet thickness to 0.65 mm sheet thickness. From the 0.65 mm to 1 mm sheet thickness the rate of change is a little higher with 54 % increase in iron losses for every 0.1 mm increase in sheet thickness whereas between 0.35 mm and 0.65 mm it is 37 %. So, from that point of view the 0.65 mm sheet would be the correct option. The efficiency requirement is fulfilled with 1 mm sheets; therefore 1 mm is good enough for the sheet thickness. Thinner sheets are also more expensive than thicker ones.

5. CONCLUSIONS

As a result of the study a rotor of a permanent magnet synchronous generator with magnets embedded inside the rotor was designed with output power of 10.4 MW. Three different rotor constructions were compared, and one fulfilled all the electrical requirements and was completely electrically designed. This study offers also knowledge and criteria for finite element analyses and modelling.

The main object of this thesis was to find out whether it is possible to build an embedded magnet rotor cost efficiently or not, when compared with a rotor-surface- magnet rotor, and to replace the previous design which has rotor-surface- magnets. The rotor design was made

for The Switch PMM1500 wind turbine generator. Design work consisted of literature review and finite element analyses.

Different analyses were done with finite element methods to design the rotor of the generator and to confirm the feasibility of the design. The machine operation and characteristics were analysed at the rated load, short circuit and no load. Analysed rotor constructions were rotors that have two magnets per pole in V-position embedded inside the rotor, tangentially embedded magnets or radially embedded magnets. The rated load analysis consisted of finding the initial values and optimization of different machine parameters. At the rated load different magnet grades were applied and cost optimum was searched for. After finding the cheapest magnet grade from the total cost point of view, the PM thickness and width was varied. As a result, it was noticed that the PM thickness has higher impact on torque production than PM width whereas the PM width has a higher impact on the torque ripple. Even though the effects of PM width on torque ripple was studied, the cheapest solution was chosen to minimize the costs. Then to improve the torque behaviour, suitable slot wedges and skewing design was applied, and the air gap length was varied. During the slot wedge design the wedge thickness and its permeability were varied. The effect on torque ripple was noticed to be small but, on the eddy current losses in the rotor, the effect was noticeable. Also, torque production was considerably weaker when the wedge thickness and permeability were increased. While choosing the air gap length, the effects on losses and torque ripple were considered. It was noticed that the air gap length has a clear effect on the rotor losses, torque ripple and PM thickness needed. Finally, the rotor surface shape was varied, and the losses and efficiencies were calculated. Shaping the rotor surface decreased the torque ripple and leakage fluxes. The main improvement was that the rotor losses were decreased as a result of decreased air-gap flux density harmonic content. After that, the pull-out torques were examined and short circuit analyses were done. With the short circuit analyses demagnetization of magnets was evaluated. Then the machine operation at no load was simulated and finally synchronous inductances were calculated.

In early phase, the radially embedded magnets design was abandoned because of the high amount of magnets, increasing costs, needed to produce desired torque. At the rated load operation both two magnets per pole in V-position and tangentially embedded magnets layouts have adequate properties. Both models can produce the needed torque with the same amount of magnet material with a 0.3 % difference in currents. The tangentially embedded magnets model has a higher efficiency and pull-out torque whereas two magnets per pole in V-position model has lower losses in PMs and a smaller torque ripple. At short circuit analyses the difference between these two designs, however, is remarkable. It was discovered that the two magnets per pole in V-position layout can be easily demagnetized. With redesigned flux barriers demagnetization characteristics improved but still with the best design the demagnetization starts at 39.9 °C with the PM material selected. This is 50.1 °C below the rotor rated temperature. With the tangentially embedded magnets layout, there should be no danger of demagnetization. Torque and current behaviours have small differences, tangentially embedded magnets layout having higher currents and torque. So, based on the results got from the finite element analysis, the tangentially embedded magnets layout is chosen to be the most suitable magnet layout for the generator. Table 5.1 lists the operational data for both the tangentially embedded magnets and two magnets per pole in V-position layouts.

Table 5.1 The operational data of tangentially embedded magnets and two magnets per pole in V-position layouts.

	tangentially embedded magnets	two magnets per pole in V-position
P_N [MW]	10.4	10.4
T_N [kNm]	254	254
U_N [V]	410	410
I_N [kA]	9.59	9.56
cos(φ) [-]	0.901	0.906
η [%]	97.8	97.7
L_d [mH]	0.051	0.055
L_q [mH]	0.055	0.082
δ [°]	51.8	68.6
T_{ripple} [%]	0.87	0.63
T_{MAX} [kNm]	375	348
I_k [kA]	11.5	10.6
PM size [mm^3]	22x68x4	22x68x7
Magnet grade	G52TH	G52TH
T_{demag} [°C]	91.9	39.9

Table 5.1 lists the main parameters of both layouts. When the properties are compared with the rotor surface magnets machine's properties, the main difference is that the embedded magnet design has a larger synchronous inductance and thus a lower torque reserve. Another significant difference is that the embedded magnet design has a higher efficiency. Originally the embedded magnet rotor was designed to be able to scale the machine for higher speeds. As the embedded magnet design offers a higher efficiency, it is better than the rotor surface magnet machine, however, the cost of magnets is 12.0 % higher with the embedded magnet design. That increase in costs will be covered in cheaper rotor construction. As the complex clamping system of magnets is removed and manufacturing labour becomes easier, the total cost of the machine does not increase. So, the PMM1500 generator can be implemented cost efficiently and with improved performance with embedded magnets.

The study was educational and succeeded to answer the research questions. It taught new things about electrical machines and their design process. Design process taught also FEM modelling of PM machines.

In a further study it would be reasonable to examine what would happen if the power of the generator would be increased. Objects of the study would be to find out how the efficiency behaves when the power is increased and what would be the maximum power that could be produced with a low-voltage machine.

REFERENCES

Aho, T., Nerg, J. & Baum, C. 2017. “Torsional Excitation Upon Short-Circuit in Induction Motors - In Conventional and High-Speed Trains.” *46th Turbomachinery and 33rd Pump Symposia (TPS 2017).*

Athanasopoulos, D., Kastros, V. & Kappatou, J. 2016. *Electromagnetic Analysis of a PMSM with Different Rotor Topologies*. Greece: Patra: University of Patras.

Charih, F., Dubas, F., Espanet, C. & Chamagne, D. 2012. “Performances Comparison of PM Machines with Different Rotor Topologies and Similar Slot and Pole Numbers.” *International Symposium on Power Electronics, Electrical Drives, Automation and Motion.*

Endo, T., Sanada, M., Morimoto, S. & Inoue, Y. 2016. “IPMSM Design to Improve Characteristics under Magnet Demagnetization.” *19th International Conference on Electrical Machines and Systems (ICEMS).*

Gieras, J. & Wing, M. 1997. *Permanent Magnet Motor Technology: Design and Applications.* New York: Dekker.

Hahlbeck, S. & Gerling, D. 2008. “Design Considerations for Rotors with Embedded V-Shape Permanent Magnets.” *18th International Conference on Electrical Machines.*

Hanna, R. & Schmitt, D. W. 2012. “Failure analysis of induction motors: Magnetic Wedges in Compression Stations.” *IEEE Industry Application Magazine.* vol. 18, issue 4, pp. 40-46.

Hendershot, J. R. & Miller, T. J. E. 1994. *Design of brushless permanent-magnet motors*. Hillsboro (OH): Oxford: Magna Physics; Clarendon Press.

Hendershot, J. R. & Miller, T. J. E. 2010. *Design of brushless permanent-magnet machines*. Venice, FL: Motor Design Books.

Kim, K., Kim, K., Kim, H. J. & Lee, J. 2009. ”Demagnetization Analysis of Permanent Magnets According to Rotor Types of Interior Permanent Magnet Synchronous Motor.” *IEEE Transactions on magnetics.*, vol. 45, no. 6.

K&J Magnetics Inc. FAQ. [Online]. [Accessed 10.2.2019]. Available at: https://www.kjmagnetics.com/faq.asp#grade

Liimatainen, T. 2015. *The Switch: Mechanical Design Manual. Company internal non-public document.*

Lindh, P., Jussila, H., Niemelä, M., Parviainen, A. & Pyrhönen, J. 2009. ”Comparison of Concentrated Winding Permanent Magnet Motors With Embedded and Surface-Mounted Rotor Magnets.” *IEEE Transactions on Magnetics.*, vol. 45, no. 5.

Lindh, P., Pyrhönen, J., Ponomarev, P. & Vinnikov, D. 2013. ” Influence of Wedge Material on Losses of a Traction Motor with Tooth-coil Windings.” *IECON 2013 - 39th Annual Conference of the IEEE Industrial Electronics Society.*

Liu, M., Pei, Y. & Shi, P. 2013. ” Optimization of Permanent Magnet Motor Air-gap Flux Density Based on the Non-uniform Air-gap.” *Proceedings 2013 International Conference on Mechatronic Sciences, Electric Engineering and Computer (MEC).*

Okamoto, J., Sanada, M., Morimoto, S. & Inoue, Y. 2013. ” Influence of Magnet and Flux Barrier Arrangement for IPMSM with Concentrated Winding.” *IEEE 10th International Conference on Power Electronics and Drive Systems (PEDS).*

Puranen, J. 2015. *The Switch: Electromagnetic Design Manual. Company internal non-public document.*

Pyrhönen, J., Jokinen, T. & Hrabovcovà, V. 2008. *Design of Rotating Electrical Machines.* Chichester: Wiley.

Pyrhönen, J., Ruoho, S., Nerg, J., Paju, M., Tuominen, S., Kankaanpää, H., Stern, R., Boglietti, A. & Uzhegov, N. 2015. ”Hysteresis Losses in Sintered NdFeB Permanent Magnets in Rotating Electrical Machines.” *IEEE Transactions on Industrial Electronics.*, vol. 62, no 2.

Salminen, P., Pyrhönen, J., Jussila, H. & Niemelä, M. 2007. ”Concentrated Wound Permanent Magnet Machines with Different Rotor Designs.” *International Conference on Power Engineering, Energy and Electrical Drives.*

Vakil, G. & Rajagopal, K. 2010. “Performance Comparison of Sinusoidally-Fed PM BLDC Motors Having Different Rotor Topologies.” *Joint International Conference on Power Electronics Drives and Energy Systems.*

Wang, A., Jia, Y. & Soong, W. 2011. “Comparison of Five Topologies for an Interior Permanent-Magnet Machine for a Hybrid Electric Vehicle.” *IEEE Transactions on Magnetics.*, vol. 47, no. 10.

Wang, S., Zhao, Z., Yuan, L. & Wang, B. 2008. “Investigation and analysis of the influence of magnetic wedges on high voltage motors performance.” Vehicle Power and Propulsion Conference, China, VPPC.

Zhao, W., Lipo, T. A. & Kwon, B. 2015. “Torque Pulsation Minimization in Spoke-type Interior Permanent Magnet Motors with Skewing and Sinusoidal Permanent Magnet Configurations.” *IEEE Transactions on Magnetics.*, vol. 51, no. 11.